IAEA-TECDOC-1649

Delayed Hydride Cracking of Zirconium Alloy Fuel Cladding

IAEA
International Atomic Energy Agency

Delayed Hydride Cracking of Zirconium Alloy Fuel Cladding

IAEA-TECDOC-1649

DELAYED HYDRIDE CRACKING OF ZIRCONIUM ALLOY FUEL CLADDING

INTERNATIONAL ATOMIC ENERGY AGENCY
VIENNA, 2010

For further information on this publication, please contact:

Nuclear Power Engineering Section
International Atomic Energy Agency
Vienna International Centre
PO Box 100
1400 Vienna, Austria
email: Official.Mail@iaea.org

Printed by the IAEA in Austria
October 2010
IAEA-TECDOC-1649

IAEA Library Cataloguing in Publication Data

Delayed hydride cracking of zirconium alloy fuel cladding. –
Vienna : International Atomic Energy Agency, 2010.
p. ; 30 cm. – (IAEA-TECDOC series, ISSN 1011-4289 ; no. 1649)
ISBN 978-92-0-108610-5
Includes bibliographical references.

1. Nuclear reactors – Materials. 2. Nuclear fuel claddings – Zirconium alloys – Hydrogen content. 3. Fuel cladding interactions.
4. Zirconium alloys – Cracking. I. International Atomic Energy Agency. II. Series.

IAEAL 10-00648

FOREWORD

This report describes the work performed in a coordinated research project on Hydrogen and Hydride Degradation of the Mechanical and Physical Properties of Zirconium Alloys. It is the second in the series. In 2005–2009 that work was extended within a new CRP called Delayed Hydride Cracking in Zirconium Alloy Fuel Cladding. The project consisted of adding hydrogen to samples of Zircaloy–4 claddings representing light water reactors (LWRs), CANDU and Atucha, and measuring the rates of delayed hydride cracking (DHC) under specified conditions. The project was overseen by a supervisory group of experts in the field who provided advice and assistance to participants as required.

All of the research work undertaken as part of the CRP is described in this report, which includes details of the experimental procedures that led to a consistent set of data for LWR cladding. The participants and many of their co-workers in the laboratories involved in the CRP contributed results and material used in this report, which compiles the results, their analysis, discussions of their interpretation and conclusions and recommendations for future work.

The research was coordinated by an advisor and by representatives in three laboratories in industrialized Member States. Besides the basic goal to transfer the technology of the testing technique from an experienced laboratory to those unfamiliar with the methods, the CRP was set up to harmonize the experimental procedures to produce consistent sets of data, both within a single laboratory and between different laboratories. From the first part of this project it was demonstrated that by following a standard set of experimental protocols, consistent results could be obtained. Thus, experimental vagaries were minimized by careful attention to detail of microstructure, temperature history and stress state in the samples.

The underlying idea for the test programme was set out at the end of the first part of the project on pressure tubes. The basic scope of the programme was formulated by the IAEA with help from the supervisory group in 2005. It was based on the materials and experimental procedures developed at the host laboratory of the CRP, Studsvik Nuclear in Sweden. The first research coordination meeting (RCM) was held in June 2005 in Nyköping, Sweden. At this RCM the test method was demonstrated and the scope of the project was confirmed. The initial specimens and test grips were ordered. Once the participants received these items, testing was started and progress was reported at the second RCM held in Pitesti, Romania, in March 2007. Other test materials donated by Canada and Argentina were delivered to the project. The third and final RCM was held in October 2008 in Daejeon, Republic of Korea, where the status of the testing was reported and final testing was decided to fill in gaps in the data. The early data were also presented at the Water Reactor Fuel Performance Meeting (WRFPM), Seoul, Republic of Korea, in October 2008, and published in a special issue of Nuclear Engineering and Technology (2009).

The IAEA wishes to thank all the participants in the CRP for their contribution to this publication. In particular, the IAEA is grateful to C.E. Coleman (Canada) who provided technical advice and programme coordination throughout the project, and to Studsvik Nuclear, Sweden, for hosting and sharing their technical expertise, arranging for the starting test materials, and organizing the first RCM. Special thanks go to the Institute for Nuclear Research in Pitesti, Romania, and to the Korea Atomic Energy Research Institute in Daejeon, Republic of Korea for organizing the second and third RCMs at their institutes. The IAEA officers responsible for this publication were P. Adelfang and V. Inozemtsev of the Division of Nuclear Fuel Cycle and Waste Technology.

CONTENTS

SUMMARY

Like other hydride-forming metals, zirconium is susceptible to embrittlement by hydrogen when hydrides are formed. The embrittlement takes two forms: short term loss of toughness and a stable, time-dependent crack growth mechanism called delayed hydride cracking (DHC). During DHC, hydrides nucleate and grow slowly in the high stress region of a stress-raiser such as a crack tip. When they reach a critical condition, probably related to size, they fracture, the crack extends and the process is repeated.

DHC has been responsible for several failures in components. Time dependent cracking was discovered during the storage at room temperature of Zr-2.5Nb fuel cladding before irradiation. High residual stresses from welding were an important factor in these fractures. Similar stresses were also responsible for cracking in Zr-2.5Nb pressure tubes. The source of these stresses was either the process used to join the pressure tube to the ends of its fuel channel or from tube straightening. Several examples show that fuel cladding made from Zircaloy is also not immune from DHC. In some Zircaloy nuclear fuel cladding used in boiling water reactors (BWR), hydride cracking was strongly implicated in long splits that allowed substantial leakage of fission products. A DHC-type of mechanism has been identified as being responsible for radial cracking starting at the outside surface of BWR fuel cladding when power ramped after a high burnup. Cracks in the axial direction, about 20 mm long and close to the end-plugs of CANDU fuel have been detected. Several partial radial cracks had also started from the inside surface. Thus DHC is of technological importance to the nuclear industry.

The two technologically relevant quantities for DHC are the critical stress intensity factor, K_I, for crack initiation, called K_{IH}, and the rate of crack propagation, called V. The latter was the subject of the first part of this IAEA Coordinated research programme (CRP) on Zr-2.5Nb Pressure Tube Material, IAEA-TECDOC-1410. As an extension of this CRP, the rate of DHC has been measured in Zircaloy–4 fuel cladding.

Several methods are available to test fuel cladding for DHC. The first such successful testing was obtained using a centre-cracked half-tube loaded in tension. To gain insight on the long splits, tubing containing a central axial crack was loaded by a wedge and mandrel - the SPLIT test. The radial crack propagation from the outside surface has been studied by internally pressurizing tubes containing small axial cracks. Axial crack propagation has been measured using the pin-loading tension (PLT) technique. This last method was chosen for the CRP programme because:

— its loading is similar to that in a compact toughness specimen used for Zr-2.5Nb in CRP-I;
— in a comparison of test methods for fracture toughness of Zircaloy–4 fuel cladding, the PLT technique provided the lowest values of crack growth resistance indicating that this technique imposes good constraint and limits plasticity at the crack tip;
— the technique was thought to be amenable to technology transfer.

The IAEA set up this extension to the CRP with the objective of transferring know-how on laboratory practices to the member states who were unfamiliar with DHC testing of fuel cladding using the PLT method. The first objective of the programme was to establish a uniform and consistent laboratory practice to determine the DHC velocity in the axial direction of fuel cladding so that a meaningful inter-laboratory comparison of the results could be made. A detailed evaluation showed that the technology transfer was successful.

Testing on a single batch of fuel cladding containing 200 ppm hydrogen showed that all laboratories obtained values of crack growth rate at 250ºC in a tight distribution with a mean value of $3.47 \times 10^{-8} \pm 0.7 \times 10^{-8}$ m/s. The temperature dependence followed Arrhenius behaviour in the temperature range 150 to 275ºC with an activation energy for V of about 53 kJ/mol. Above 275ºC, the cracking rate declined and eventually stopped when the temperature reached 290ºC.

The second objective of the programme was to examine the effects of microstructure on V. Six versions of Zircaloy–4 fuel cladding were tested, ranging from as cold worked to fully annealed materials. The materials represented materials used in PWR, BWR, CANDU and Atucha. The results showed that:

— The cracking rate was independent of crack length and therefore stress intensity factor.
— The temperature dependencies of cracking were similar in cold worked and stress relieved materials.
— The cracking in annealed material was very variable and it may have been tested close to its threshold stress intensity factor, $K_{IH.}$
— Material strength was a controlling factor for V, with cracking being fastest in the strongest material.
— Crystallographic texture was not as important as had been previously thought; fuel cladding has a strong radial texture, which was thought to suppress DHC, but the materials cracked readily.
— The fractographic feature called striations, which are so dominant in the DHC of Zr-2.5Nb, were absent indicating that they are not a fundamental characteristic of DHC in Zircaloy.
— The decline in V at high temperatures is attributed to K_{IH} rapidly increasing with temperature around 280ºC and eventually being higher than the applied stress intensity factor.

During the project advanced techniques for measurements of the rate of DHC propagation in cladding zirconium alloys were successfully transferred from the host laboratory (Studsvik Nuclear) to all participating organizations, and a statistically valuable set of experimental results was obtained by following the pre-agreed testing procedures. The results contributed to better understanding of the DHC phenomenon and were reported at a number of international conferences including WRFPM-2008 and ASTM Zr Symposium 2010. They have stimulated some national programmes that are useful as a base for interpreting the behaviour of irradiated materials and for the application of post-service fuel storage.

Another technologically important DHC parameter, the critical stress intensity factor for crack initiation K_{IH}, is recommended for further studies in both Zr-2.5Nb pressure tube materials and Zircaloy fuel cladding. Such new project would exploit the experience built-up over the past eight years of IAEA-coordinated research activities targeting the mechanisms of hydrogen induced degradation of operational properties of zirconium materials.

CHAPTER 1

INTRODUCTION

Zirconium is the main base metal for alloys used as fuel cladding and structural components in water cooled nuclear reactors. These alloys have low capture cross-sections for thermal neutrons, maintain good mechanical properties both during and after irradiation with fast neutrons, and resist corrosion. Zirconium alloys have provided excellent service but, like other hydride-forming metals, zirconium is susceptible to embrittlement by hydrogen when hydrides are formed [1.1]. The embrittlement takes two forms: short term loss of toughness and a stable, time-dependent crack growth mechanism called delayed hydride cracking (DHC).

During DHC, hydrides nucleate and grow slowly in the high stress region of a crack tip. When they reach a critical condition, probably related to size, they fracture, the crack extends and the process is repeated. The characteristics of the mechanism are:

— Often time is required between the imposition of stress and the start of cracking. This period is called the incubation time.
— Loading must exceed a threshold condition for cracking, often characterized as K_{IH}. The rate of any subsequent cracking, V, is almost independent of K_I.
— The temperature dependence of cracking is complicated and is described in the schematic diagram depicted in Fig. 1.1 (Ref [1.2]). The maximum value of V has an apparent Arrhenius behaviour and follows

$$V = A \cdot \exp(-Q/RT) \qquad (1.1)$$

where Q is the activation energy for DHC in kJ/mol, R is the gas constant (8.314 kJ/mol·K), and T is the temperature in K and A is a constant.

If the temperature is attained by heating from T_1, initially V follows Equation (1.1) but as the temperature is increased, V starts to decline at T_2 and cracking eventually stops at T_3. On cooling from a high temperature, T_4, a temperature is reached where cracking will reinitiate, T_5, and reach a maximum value at T_6; at lower temperatures V follows Equation (1.1).

— The amount of hydrogen present in the material should be sufficient for hydrides to be precipitated at the crack tip.
— The material microstructure may affect V through its effect on the diffusivity of hydrogen, material strength and mode of hydride precipitation, for example, through crystallographic texture.
— A sharp decline in DHC is observed at high test temperatures, despite the temperature being attained by cooling and sufficient hydrogen being present to form hydrides. In Zr-2.5Nb the decline starts at about 310ºC [1.3].

In the early development of the alloys of titanium, an element in the same group as zirconium in the Periodic Table, a form of DHC was a scourge to their application but zirconium alloys were thought to be immune. Attempts to induce DHC in Zircaloy-2,

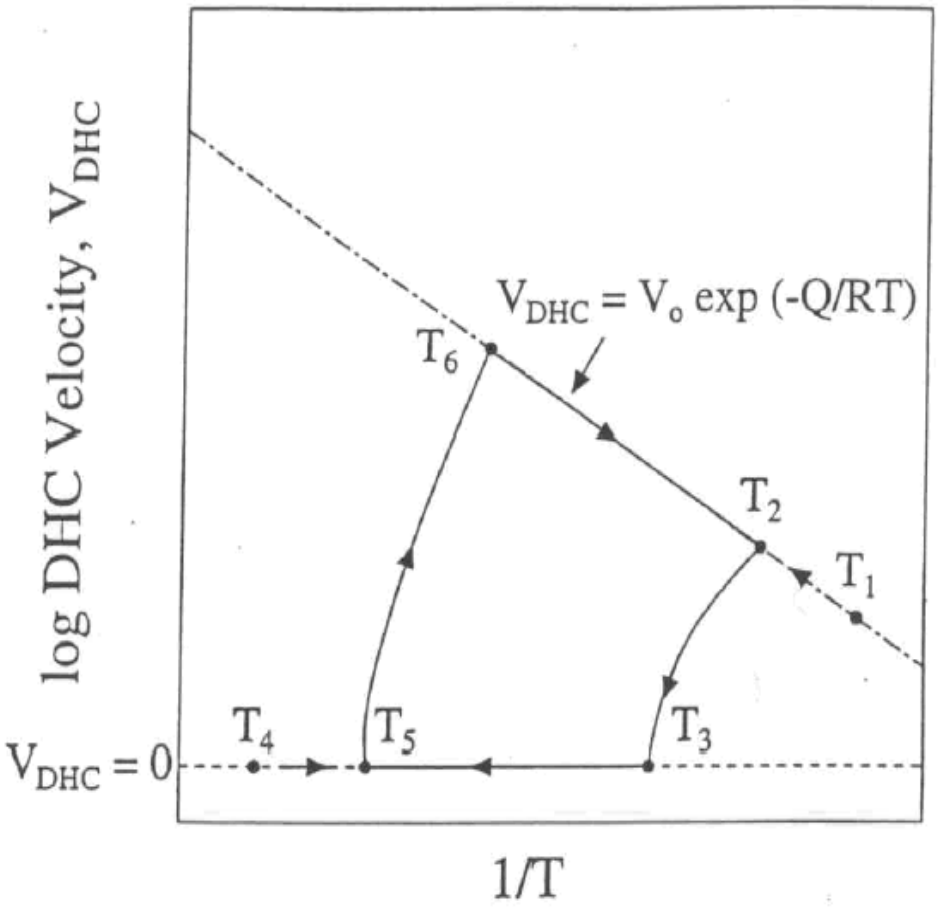

FIG. 1.1. Schematic diagram of temperature dependence of DHC in zirconium alloys [1.2]. The conditions for testing are aimed at being below T_6.

Zr-2.5Nb and Zr-1.25Al-1Sn-1Mo seemed to indicate that such cracking was difficult [1.4, 1.5]. Time dependent cracking was discovered during the storage at room temperature of Zr-2.5Nb fuel cladding before irradiation [1.6]. High residual stresses from welding were an important factor in these fractures. High residual stresses were also responsible for cracking in Zr-2.5Nb pressure tubes. The source of these stresses was either the process used to join the pressure tube to the ends of its fuel channel [1.7] or from tube straightening [1.8]. DHC was the mechanism for propagation of cracks formed at hydride blisters in Zircaloy-2 pressure tubes [1.9]; here a large temperature gradient contributed to the accumulation of hydrides at the crack tip.

In some Zircaloy nuclear fuel cladding used in boiling water reactors (BWR), hydride cracking was strongly implicated in long splits that allowed substantial leakage of fission products [1.10, 1.11, 1.12]. Cladding in BWRs is usually a tube with diameter of about 10 mm, wall thickness of about 0.6 mm and length of about 4 m. The Zircaloy is usually recrystallized and in some designs of fuel rod the inside surface is lined with another zirconium alloy or pure zirconium, to prevent stress corrosion cracking by fission products, such as iodine [1.13]. If the cladding wall is penetrated during operation, for example by fretting, water from the heat-transport system can enter the fuel cavity where, because of the low pressure, steam is produced. Much hydrogen is generated because the steam oxidizes the fuel and the inside surface of the cladding, reducing the partial pressure of oxygen and leaving a gas rich in hydrogen. This process is called ‘oxygen starvation’. At some distance from the

primary defect the gas stream becomes almost pure hydrogen, and with break down of the protective oxide layer, copious quantities of hydrogen may be absorbed by the cladding [1.14]. Sometimes, 'sunbursts' of hydride formed on the inside surface. Although the pure Zr liner was often found to be completely corroded and therefore contributed hydrogen to the inventory and stress through expansion via the oxide, it was not a necessary requirement for the secondary damage because unlined fuel cladding behaved in a similar manner. With fuel expansion during fuel rearrangement, the hydrided cladding was stressed, which led to crack initiation. The cracks grew through-wall, propagated axially, and could be over 1 m long. Brittle regions in "chevrons" characterized the fractures, with the crack being longer on the outside surface than the inside surface of the cladding [1.15]. The lower bounds of the crack velocities were in the range 4×10^{-8} to 6.6×10^{-7} m/s based on assuming constant growth rates in the time between first detection of the defect and removal of the fuel. The mechanism of cracking appeared to be a form of DHC [1.11, 1.16], perhaps exacerbated by a continuous additional supply of hydrogen from the steam inside the fuel element [1.17, 1.18].

A DHC-type of mechanism has been identified as being responsible for radial cracking starting at the outside surface of BWR fuel cladding when power ramped after a high burnup [1.19]. Tests on unirradiated cladding demonstrated that the velocity of DHC in the radial direction of the tube obeyed equation (1.1) and V was about 10^{-7} m/s at 275ºC [1.20, 1.21].

The two technologically important quantities for DHC are the conditions for crack initiation and the rate of crack propagation. The latter was the subject of the first part of this IAEA CRP. The details of the results of testing on Zr-2.5Nb pressure tube material and a state of the art review were issued in an IAEA-TECDOC-1410[1.22] and summarised in Ref [1.23]. As an extension of this CRP, the rate of DHC has been measured in Zircaloy fuel cladding.

Several methods are available to test fuel cladding for DHC. The first such successful testing was obtained using a centre-cracked half-tube loaded in tension [1.24]. To gain insight on the long splits, tubing containing a central axial crack was loaded by a wedge and mandrel — the SPLIT test [1.17]. The radial crack propagation from the outside surface has been studied by internally pressurizing tubes containing small axial cracks [1.20, 1.21]. Axial crack propagation has been measured using the pin-loading tension (PLT) technique [1.25]. This last method was originally developed at Studsvik for fracture toughness evaluation of thin walled tubing [1.26, 1.27] and was chosen for the CRP programme because:

— Its loading is similar to that in a compact toughness specimen used in CRP I;
— In a comparison of test methods for fracture toughness of Zircaloy–4 fuel cladding, the PLT technique provided the lowest values of $J_{0.2}$ and dJ/da indicating that this technique provides good constraint and limits plasticity at the crack tip [1.28];
— The technique was thought to be amenable to technology transfer, especially since an established member of the CRP developed the method.

The IAEA set up this extension to the CRP on Hydrogen and Hydride-Induced Degradation of the Mechanical and Physical Properties of Zirconium-based Alloys, with the objective of transferring know-how on laboratory practices to the member states who participated in the first stage of the CRP but were unfamiliar with DHC testing of fuel cladding using the PLT method. The participants in this stage of the CRP are listed in Table 1.1; Brazil replaced China as a participant. The major goal of the programme was to establish a uniform and consistent laboratory practice to determine the DHC velocity in the axial direction of fuel cladding to be followed internationally so that a meaningful inter-laboratory comparison of the results could be made. The test materials were all versions of Zircaloy–4.

In this report, Chapter 2 describes the materials, specimen preparation and test methods, the test results are displayed in Chapter 3 and discussed in Chapter 4, while in Chapter 5 conclusions and recommendations are made.

TABLE 1.1. PARTICIPATING COUNTRIES AND THEIR REACTOR TYPES OF INTEREST

INSTITUTE[1]	COUNTRY	REACTOR TYPE
CNEA	Argentina	CANDU, PWR (D_2O moderated)
IPEN	Brazil	PWR
AECL	Canada	CANDU
BARC	India	CANDU
KAERI	Korea, Rep. of	CANDU, PWR
LEI	Lithuania	RBMK
PINSTECH	Pakistan	CANDU
INR	Romania	CANDU
VNINM	Russian Federation	RBMK, WWER
STUDSVIK	Sweden	BWR, PWR, surveillance on RBMK

REFERENCES TO CHAPTER 1

[1.1] COLEMAN, C.E., Cracking of hydride-forming metals and alloys, Comprehensive Structural Integrity, Elsevier, Chapter 6.03, (2003), 103–161.

[1.2] CHEADLE, B.A., COLEMAN, C.E., AMBLER, J.F.R., Prevention of delayed hydride cracking in zirconium alloys, Zirconium in the Nuclear Industry – Seventh International Symposium, ASTM STP **939**, Philadelphia, PA., (1987), 224–240.

[1.3] SMITH, R.R., EADIE, R.L., High temperature limit for delayed hydride cracking, Scripa Met., **22**, (1988), 833–836.

[1.4] ÖSTBERG, G., Some observations on the ductility of zirconium alloys, with special reference to the effect of hydrogen, J. Inst. Metals, **93**, (1964-65), 223–228

[1.5] WEINSTEIN, D., HOLTZ, F.C., Susceptibility of zirconium and zirconium alloys to delayed failure hydrogen embrittlement, Trans. ASM. **57**, (1964), 284–293.

[1.6] SIMPSON, C.J., ELLS, C.E., Delayed hydrogen embrittlement of Zr-2.5wt%Nb J. Nucl. Mater. **52**, (1974), 289–295.

[1.7] PERRYMAN, E.C.W., Pickering pressure tube cracking experience, Nucl. Energy **17**, (1978), 95–105.

[1.8] PLATONOV, P.A., et al, The study of cause of cracking in zirconium alloy channel tubes, Poster Paper at ASTM Zirconium in the Nuclear Industry – Eighth International Symposium, AECL Report RC **87**, (1988).

[1.9] FIELD, G.J., DUNN, J.T., CHEADLE, B.A., Analysis of the pressure tube failure at pickering NGS “A” unit 2, Can. Met. Quart. **24**, (1985), 181–188.

[1] The names of the contributing persons are given at end of this publication.

[1.10] JONSSON, A., HALLSTADIUS, L., GRAPENGIESSER, B., LYSELL, G., Failure of a barrier rod in Oskarshamn, in Fuel in the '90's, International Topical Meeting on LWR Fuel Performance, Avignon, France, ANS and ENS, (1991), 371–377.
[1.11] SCHRIRE, D., et al, Secondary defect behaviour in ABB BWR fuel, International Topical Meeting on LWR Fuel Performance, West Palm Beach, ANS, (1994) 398–409.
[1.12] ARMIJO, J.S., Performance of failed BWR fuel, International Topical Meeting on LWR Fuel Performance, West Palm Beach, ANS, (1994), 410–422.
[1.13] ARMIJO, J.S., COFFIN, L.F., ROSENBAUM, H.S., Development of zirconium-barrier fuel cladding, Zirconium in the Nuclear Industry – 10th International Symposium, ASTM STP **1245**, ASTM, West Conshohocken, PA, (1994), 3–18.
[1.14] CLAYTON, J.C., Internal hydriding in irradiated defected zircaloy fuel rods, Zirconium in the Nuclear Industry – 8th International Symposium, ASTM **1023**, West Conshohocken, PA, (1989), 266–288.
[1.15] LYSELL, G., GRIGORIEV, V., Characteristics of axial splits in failed BWR fuel rods, Ninth International Symposium on Environment Degradation of Materials in Nuclear Power Systems – Water Reactors, AIME-TMS, (1999), 1.169–1.175.
[1.16] EFSING, P., PETTERSSON, K., Delayed hydride cracking in irradiated Zircaloy cladding, Zirconium in the Nuclear Industry – 12th International Symposium, ASTM STP **1354**, West Conshohocken, PA., (2000), 340–355.
[1.17] EDSINGER, K., DAVIES, J.H., ADAMSON, R.B., Degraded fuel cladding fractography and fracture behavior, Zirconium in the Nuclear Industry – 12th International Symposium, ASTM STP 1354, G.P. Sabol and G.D. Moan, Eds., ASTM, West Conshohocken, PA., (2000), 316-339.
[1.18] EDSINGER, K., A review of fuel degradation in BWRs, Int. Topical Meeting on Light Water Reactor Fuel Performance, Park City, ANS, (2000), 162–179.
[1.19] SHIMADA, S., ETOH, E., HAYASHI, H., TUKUTA, Y., A metallographic and fractographic study of outside-in cracking caused by power ramp tests, J. Nucl. Mater. **327**, (2004), 97–113.
[1.20] SAKAMOTO, K., NAKATSUKA, M., HIGUCHI, T., Simulation of cracking during outside-in type failure of high burn-up fuel cladding tubes, Water Reactor Fuel Performance Meeting, Seoul, (2008), Paper 8009.
[1.21] OGATA, K., BABA, T., KAMIMURA, K., ETOH, Y., ITO, K., Separate effects of factors affecting outside-in cracking of high burnup fuel cladding, Water reactor fuel performance meeting, Seoul, (2008), Paper 8130.
[1.22] INTERNATIONAL ATOMIC ENERGY AGENCY, Delayed hydride cracking in zirconium alloys in pressure tube nuclear reactors, IAEA-TECDOC-1410, IAEA, Vienna (2004).
[1.23] COLEMAN, C.E., INOZEMTSEV, V.V., Measurement of rates of delayed hydride cracking (DHC) in Zr-2.5 Nb alloys – an IAEA Coordinated Research Project, J. ASTM International **5**, (2008), Paper JAI101091.
[1.24] EFSING, P., PETTERSSON, K., The influence of temperature and yield strength on delayed hydride cracking in hydrided Zircaloy-2, Zirconium in the Nuclear Industry – Eleventh International Symposium, ASTM STP **1295**, Philadelphia, PA., (1996), 394–404.
[1.25] GRIGORIEV, V., JAKOBSSON, R., Delayed hydride cracking velocity and J-integral measurements on irradiated BWR cladding, J.ASTM International **2**, (2005), Paper JAI 12434 (Also see ASTM STP **1467**, (2006), 711–728).

[1.26] GRIGORIEV, V., JOSEFSSON, B., LIND, A., ROSBORG, B., A Pin-Loading Tension test for evaluation of thin-walled tubular materials, Scripta Metallurgica et Materialia, Vol. **33**, No. 1, (1995), 109–114.
[1.27] GRIGORIEV, V., JOSEFSSON, B,. ROSBORG, B., Fracture toughness of Zircaloy cladding tubes, Zirconium in the Nuclear Industry – Eleventh International Symposium, ASTM STP **1295**, Philadelphia, PA., (1996), 431–447.
[1.28] YAGNIK, S.K., ET AL., Round-robin testing of fracture toughness characteristics of thin-walled tubing, J. ASTM International **5**, (2008), Paper JAI101140.

CHAPTER 2

EXPERIMENTAL PROGRAMME

2.1. PHILOSOPHY OF TESTING PROGRAMME

The programme was set up using the previous CRP on Zr-2.5Nb as a guide. For the first phase the host laboratory, Studsvik (Sweden), supplied test fixtures, two fully prepared samples and a section of the same fuel cladding for each country to prepare specimens in their own each laboratory. Everyone tested several of these specimens at a single temperature, 250ºC, to establish the technique and solve any experimental problems. The remaining material was tested at other temperatures prescribed by a test matrix. For the second phase, similar cladding, but from a different batch, was taken after final cold pilgering. This cladding was heat-treated in the laboratory at the temperatures and times typical for PWR and BWR cladding. These three materials — as-cold worked, stress relieved, and fully recrystallized — were then hydrided and tested at the same temperatures as in the first phase. Subsequently, in a third phase, a small number of tests were done on two representative samples of CANDU and one sample of Atucha fuel cladding. All the specimens contained about 200 ppm to represent a concentration well towards the end of life of BWR fuel rods and to guarantee that hydrides are present throughout testing.

2.2.MATERIALS

The material used for Phase 1 was standard Zircaloy–4 from Sandvik lot 86080. The main elements in the chemical composition are given in Table 2.1. During fabrication the final pilgering imposed 80% cold-work, based on area reduction on a cylindrical mandrel, and the final heat-treatment was 480ºC for 3.5 h. The tube dimensions are listed in Table 2.2. The microstructure consisted of elongated grains, with between 5 and 10% recrystallised grains and Zr-$(FeCr)_2$ second phase particles, Fig. 2.1. The (0002) pole figure is shown in Fig. 2.2. The basal plane normals were concentrated about 30º from the radial direction; the texture factors, F, in the three principal directions, radial, R, transverse, T, and axial, A, are summarised in Table 2.3. The tensile properties of the tubes are provided in Table 2.4.

For Phase 2 the material was similar, being Zircaloy–4 fuel cladding from Sandvik lot 83786. The small difference in chemical composition was a slightly higher concentration of oxygen than in lot 86080, Table 2.1. The material was tested in the cold worked condition. Sections of tubing were also heat-treated to simulate that used for PWRs — 480ºC for 3.5 h — and for BWRs —565ºC for 1.5 h. Since the material for Phase 2 was taken from the manufacturing route direct after final pilgering, its wall thickness was slightly larger than that of lot 86080, Table 2.2. The initial cold worked microstructure consisted of elongated grains, Fig. 2.3, that were little changed by the stress-relieving treatment, Fig. 2.4, but completely recrystallized by the higher temperature anneal, Fig. 2.5, with grains that are almost equiaxed having a mean diameter of about 3 μm.

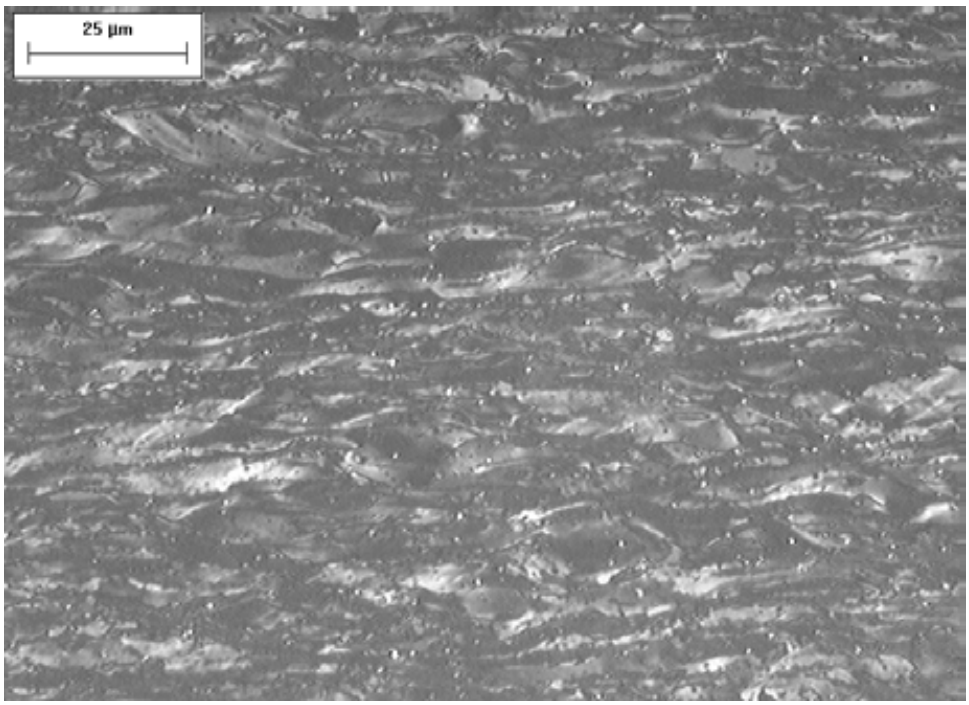

FIG. 2.1. Microstructure of Zircaloy–4 from Lot 86080. (Radial direction of the tube is vertical on the page and the longitudinal direction is horizontal).

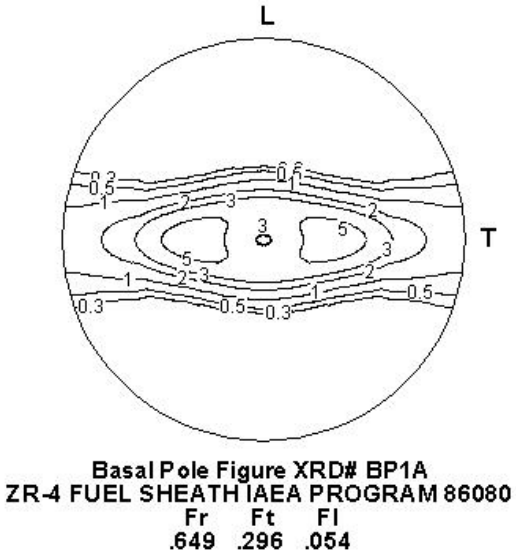

FIG. 2.2. Basal pole Figure for lot 86080 test material: Zircaloy–4 in cold worked and stress relieved condition.

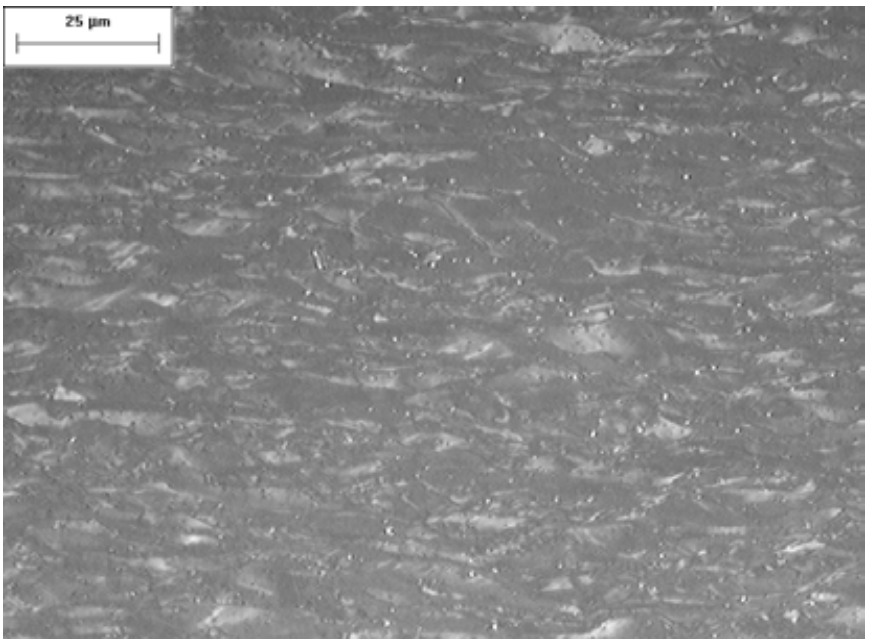

FIG. 2.3. Microstructure of Zircaloy–4 from Lot 83786 in the cold worked condition (Radial direction of the tube is vertical on the page and the longitudinal direction is horizontal).

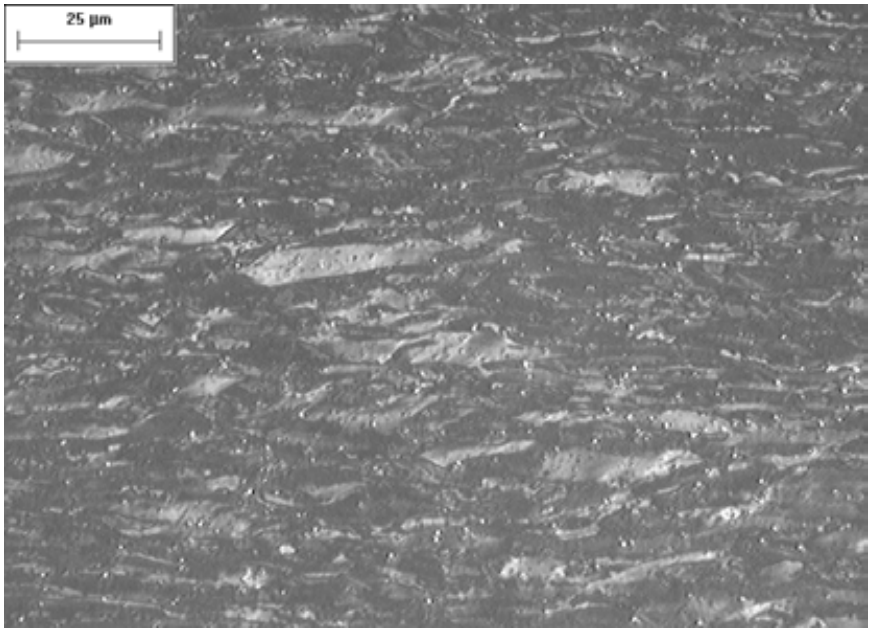

FIG. 2.4. Microstructure of Zircaloy–4 from Lot 83786 in the cold worked and stress relieved condition (Radial direction of the tube is vertical on the page and the longitudinal direction is horizontal).

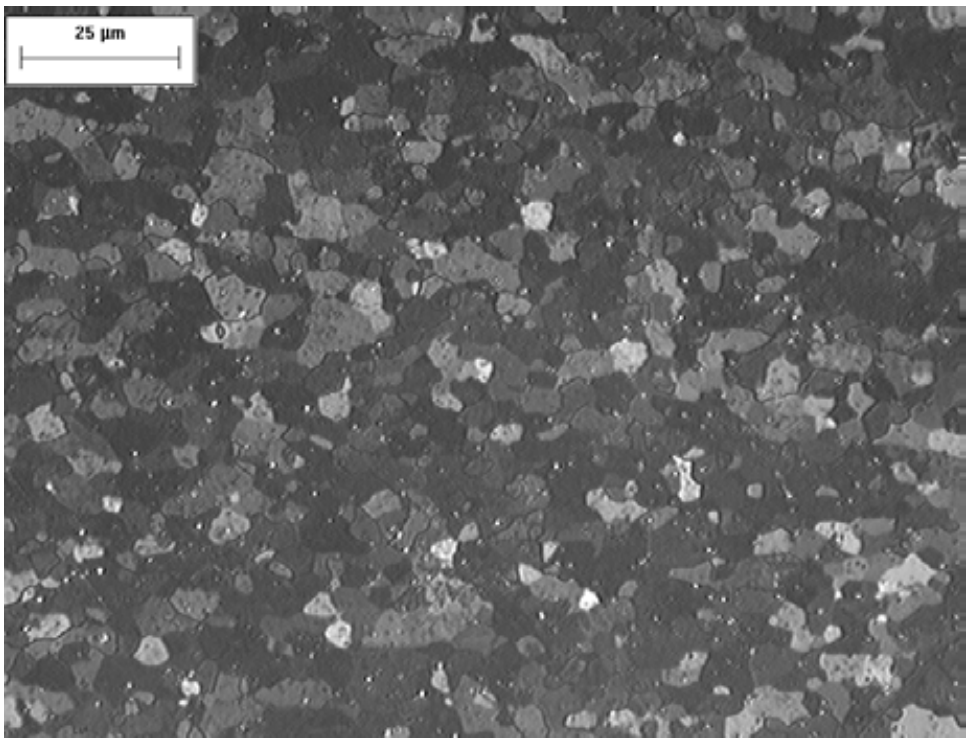

FIG. 2.5. Microstructure of Zircaloy–4 from Lot 83786 in the recrystallized condition (Radial direction of the tube is vertical on the page and the longitudinal direction is horizontal).

The (0002) pole figures for each treatment are similar, Figs. 2.6 to 2.8, with a small rotation from the radial direction towards the transverse direction with heat-treatment, as indicated by the texture factors, Table 2.3. The strength is reduced by heat-treatment, Table 2.4. Note that these strengths do not include the effect of the treatment to add hydrogen.

TABLE 2.1. CHEMICAL COMPOSITION OF TEST MATERIALS

Materials					
Element	PWR	PWR	CANDU	CANDU	Atucha
	Sandvik	Sandvik	Zircatec	Sandvik	FAE
	Lot 86080	Lot 83786	Lot 226289	Lot 81101	Lot MA-61
Sn (wt.%)	1.25	1.26	1.3	1.35	1.29
Fe (wt.%)	0.22	0.23	0.22	0.22	0.23
Cr (wt.%)	0.1	0.12	0.12	0.10	0.12
O (ppm)	1180	1272	1180	1260	1200
Si (ppm)	100	100	100	60	98
C (ppm)	120	120	140	120	132
N (ppm)	49	41	24	<30	28
H (ppm)	7	7	8	13	4

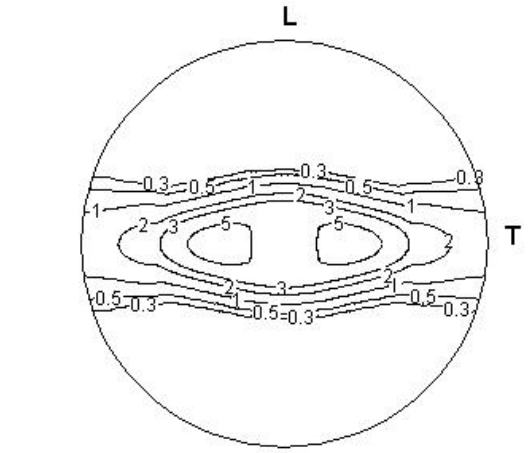

FIG. 2.6. Basal pole Figure for Lot 83786 test material in the cold worked condition.

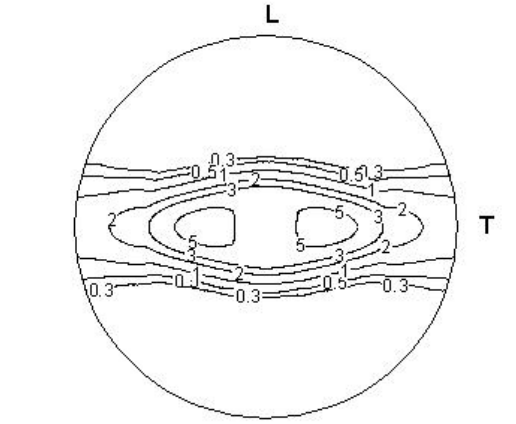

FIG. 2.7. Basal pole Figure for Lot 83786 test material in the cold worked and stress relieved condition.

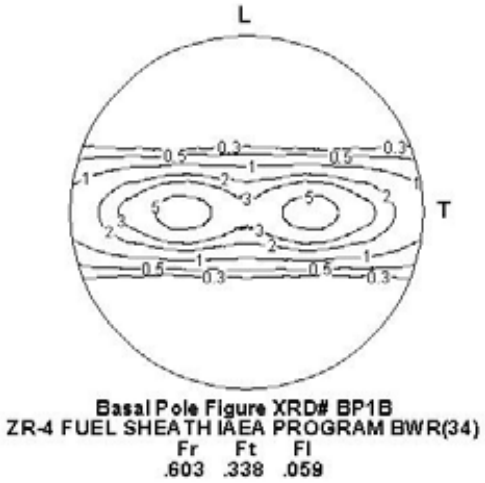

FIG. 2.8. Basal pole Figure for Lot 83786 test material in the recrystallized condition.

Three other batches of cladding were used in Phase 3. For the CANDU cladding supplied by Zircatec, the last stage of cold working was about 90% and the final stress relieving was 500ºC for 8 h. The composition of the Zircaloy–4, Table 2.1, and the (0002) distribution, Fig. 2.9 and Table 2.3, were similar to those of the LWR cladding. The dimensions of the CANDU cladding differ from the LWR cladding having a larger diameter and thinner wall, Table 2.2. It also has lower strength, Table 2.4. The clearly defined grains were elongated in the axial direction, Fig. 2.10, but almost equiaxed on the transverse-radial section, Fig. 2.11, with a mean grain diameter of about 4 μm.

For the CANDU cladding supplied by Sandvik, the composition of the Zircaloy–4 is given in Table 2.1. This CANDU cladding also differs from the LWR cladding having a larger diameter and thinner wall, Table 2.2, and lower strength, Table 2.4. The grain size was about 5.8 μm on the transverse-radial section but elongated in the longitudinal direction.

For the Atucha cladding, the last stage of cold-working was 57% and the final stress relieving was 510ºC for 8.5 h. The composition of the Zircaloy–4, Table 2.1, and the (0002) distribution, Table 2.3, again were similar to those of the LWR cladding. The Atucha cladding has a larger diameter but similar wall thickness as the LWR cladding, Table 2.2, and lower strength, Table 2.4. The clearly defined grains were elongated in the axial direction, but almost equiaxed on the transverse-radial section, with a mean grain diameter of about 2 μm in the radial direction and 3 μm in the transverse direction.

TABLE 2.2. DIMENSION OF TEST MATERIALS

Materials					
Dimensions	PWR	PWR	CANDU	CANDU	Atucha
	Sandvik	Sandvik	Zircatec	Sandvik	FAE
	Lot 86080	Lot 83786	Lot 226289	Lot 81101	Lot MA-61
Outside diameter	9.5	9.5	13.1	13.1	11.9
(mm)					
Wall thickness	0.57	0.60	0.39	0.39	0.55
(mm)					

TABLE 2.3. TEXTURE FACTORS FOR BASAL PLANES IN TEST MATERIALS

Materials						
Texture	PWR	PWR	PWR	PWR	CANDU	Atucha
factors	Sandvik	Sandvik	Sandvik	Sandvik	Zircatec	FAE
	Lot 86080	Lot 83786	Lot 83786	Lot 83786	Lot 226289	Lot MA-61
	CWSR	CW	CWSR	RXA		
F_R	0.65	0.65	0.64	0.60	0.65	0.56
F_T	0.30	0.29	0.30	0.34	0.30	0.29
F_L	0.05	0.06	0.05	0.06	0.05	0.15

TABLE 2.4. TENSILE PROPERTIES OF TEST MATERIALS

Material	Test Direction	Test	0.2%	UTS	Total
	L: longitudinal	Temperature	Stress		Elongation
	T: transverse	(ºC)	(MPa)	(MPa)	(%)
PWR	L	20	553	758	19
Sandvik	L	385	355	448	20
Lot 86080	T	200		541	
CWSR	T	200		544	
480 C for 3.5 h +	T	250		502	
410 C for 24 h	T	290		480	
	T	290		474	
	T	320		459	
PWR	T	200		588	
Sandvik	T	250		535	
Lot 83786	T	250		529	
CW	T	290		498	
	T	320		478	
	T	320		473	

TABLE 2.4. (cont.)

PWR	L	20	589	779	16
Sandvik	L	385	370	466	17
Lot 83786	T	200		570	
CWSR	T	250		508	
480 C for 3.5 h	T	250		511	
	T	290		489	
	T	320		469	
	T	320		462	
PWR	T	25		526	
Sandvik	T	25		507	
Lot 83786	T	250		270	
RXA	T	350		228	
565 C for 1.5 h					
CANDU	L	20	487	615	30
Zircatec	T (burst test)	20	…	868	24
Lot 226289	T	22	512	609	35.6
500 C for 8 h	T	22	492	602	42.4
	T	100	448	507	45.7
	T	100	441	510	43.3
	T	200	391	416	48.7
	T	200	375	414	42.9
	T	300	345	373	49.7
	T	300	303	368	52.1
	T	350	301	346	43.5
	T	350	299	345	34.4
Material	Test Direction	Test	0.2%	UTS	Total
	L: longitudinal	Temperature	Stress		Elongation
	T: transverse	(ºC)	(MPa)	(MPa)	(%)
CANDU	L (Tube tensile)	20	470	580	32
Sandvik	T (burst test)	20	…	760	31
Lot 81101	T	20	498	589	18
	T	250	300	424	20
Atucha	L	20	460	584	27
FAE	T	20		557	
Lot MA-61	T	20		594	
	T	200		412	
	T	200		399	
	T	250		362	
	T	250		372	
	T	300		348	
	T	300		344	

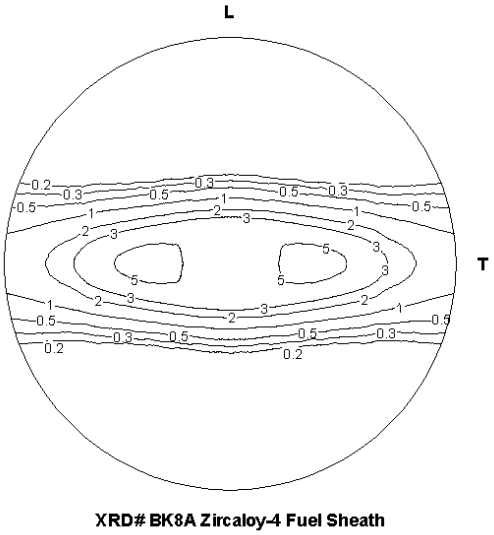

FIG. 2.9. Basal pole Figure for CANDU Lot 226289 test material in the cold worked and stress relieved condition.

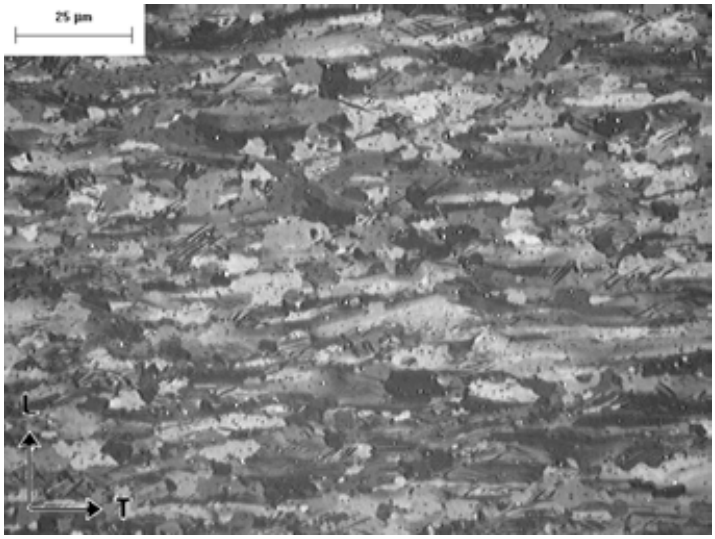

FIG. 2.10. Microstructure of Zircaloy–4 from CANDU Lot 226289 in the cold worked and stress relieved condition; longitudinal section.

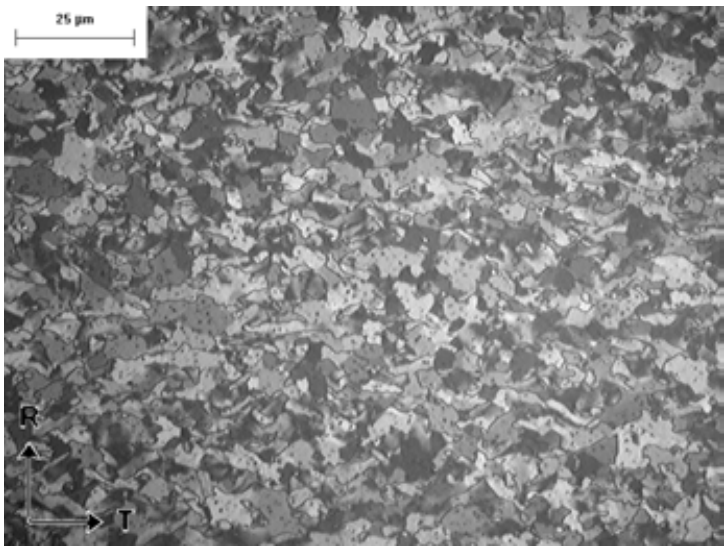

FIG. 2.11. Microstructure of Zircaloy–4 from CANDU Lot 226289 in the cold worked and stress relieved condition; transverse section.

2.3. SPECIMEN AND FIXTURE PREPARATION

The basic procedure for testing is given in [2.1, 2.2]. After cleaning, a layer of hydride was deposited on the surfaces electrolytically using 0.1 molar H_2SO_4, a temperature of 65 ± 5ºC and a current density of 1 kA/m^2. Diffusing the hydrogen in to the metal by annealing at 410 °C for 24 h added a homogeneous hydrogen concentration of about 200 ppm. The resulting hydrides had plate normals in the radial direction, Fig. 2.12, in the materials with elongated grains. The hydrogen concentration was confirmed by analysis, usually using an inert gas fusion technique. For a few specimens the hydrogen was added gaseously at 400ºC, with similar results.

The test specimen is shown in Fig. 2.13. The 13 mm long specimen (c_A) contained diametrally opposite axial notches at both edges with those at one end being sharpened by fatigue at room temperature for a starting length of a_A; the notch at the other end provided an effective specimen length of b_A. The notch that was fatigued to a crack was 0.15 mm wide while the rear notch was 0.5 mm wide. The fatigue pre-cracking was done at 1 to 5 Hz with starting maximum loads of 200 to 300 N cycled down to 50 N. The maximum load was gradually reduced to 90 to 100 N as the crack progressed. The final load was chosen to be lower than the starting load for the DHC test, typically 160 N, so the plastic zone at the crack tip from fatigue did not interfere with DHC. Between 8000 and 50 000 cycles were required to produce a suitable starting crack, about 1.5 mm in length. The crack length was measured either visually on the surface or using potential drop. In a few specimens the starter crack could not be made by fatigue and DHC was started from as sharp a notch as possible. The scatter in results from these specimens was larger than in those that were started from a fatigue crack.

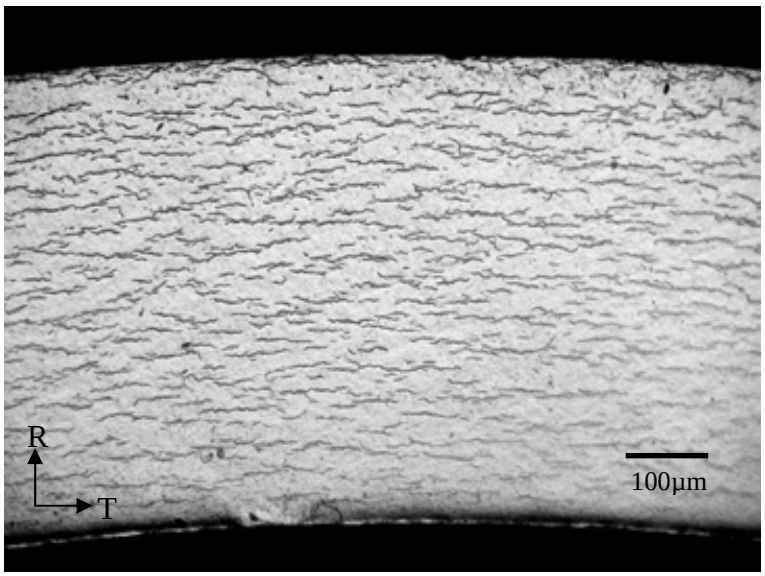

a

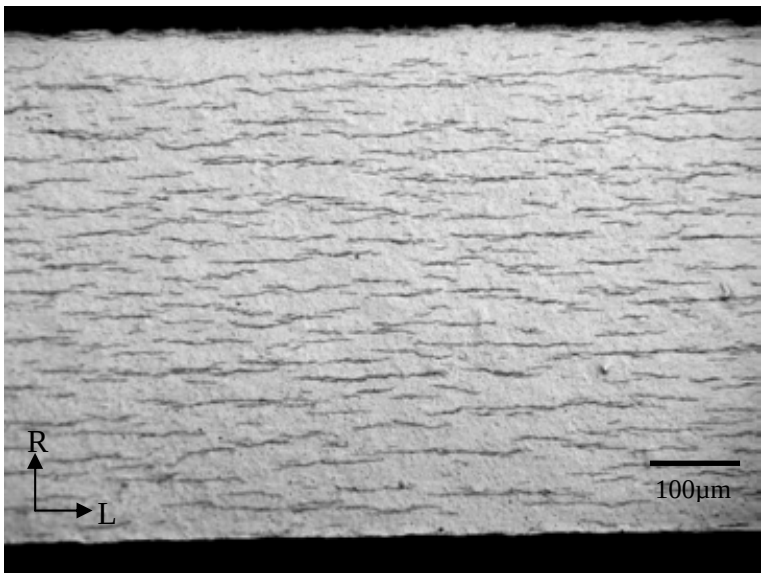

b

FIG. 2.12. Distribution of hydrides on (a) transverse-radial plane, and (b) longitudinal-radial plane. Lot 86080 in CWSR condition.

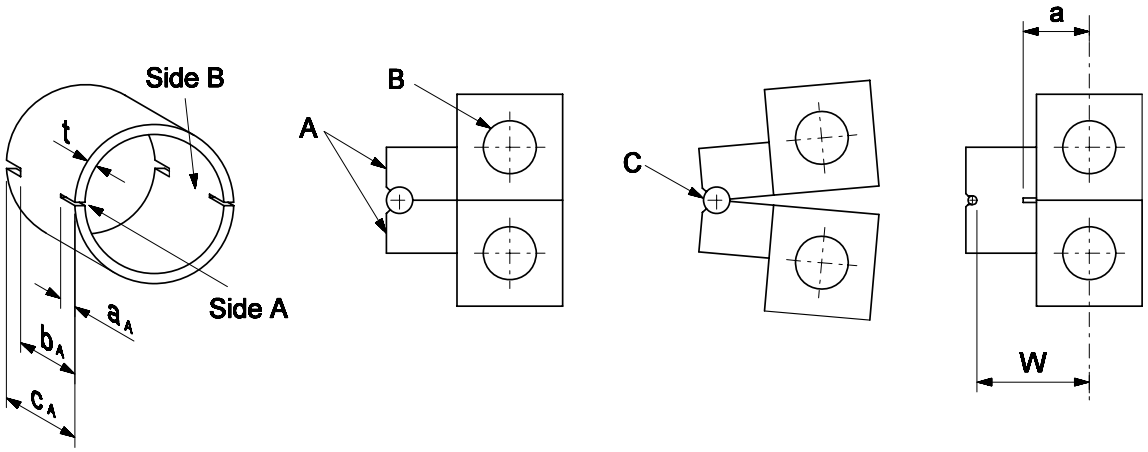

FIG. 2.13. Schematic diagram of test specimen and pin-loading tension fixture.

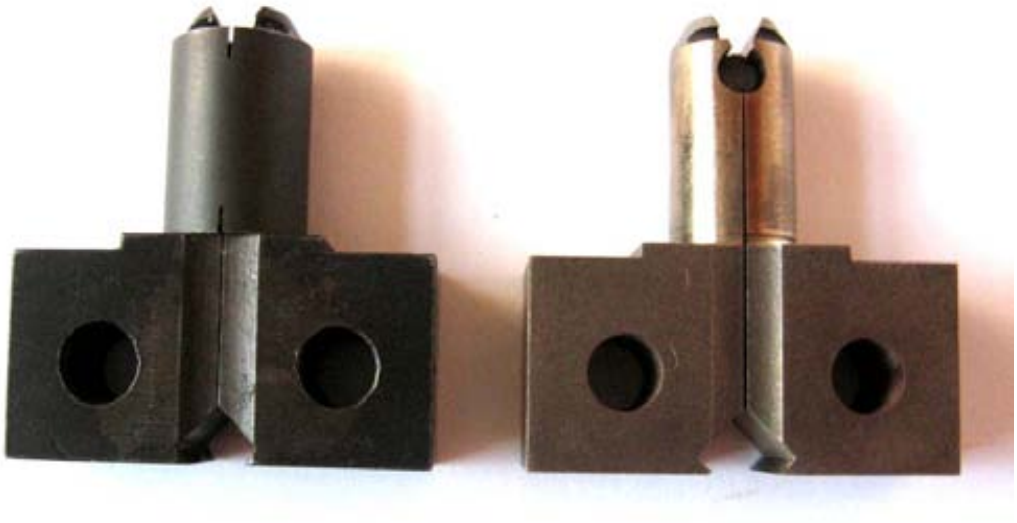

FIG. 2.14. The PLT fixture; a specimen is in place on the left side.

The pin-loading tension fixture is shown schematically in Fig. 2.13 and in a photograph in Fig. 2.14. Most of the fixtures were made from Nimonic 90 but successful testing has been achieved using fixtures made from carbon steel. The fixture consisted of two halves, which, when placed together, form a cylindrical holder, A**.** The diameter of the holder allowed it to be inserted into the specimen while maintaining a small gap. The fixture halves were loaded in tension through pins at B and rotated about a pin C at the ends of the cylindrical holder providing similarity to the loading of a compact toughness specimen, but on two cracks. Care was taken to line up the pre-cracked notches with the join of the two halves of the fixture.

2.4. DHC TESTING

To start a DHC test, the specimen was heated to and held at a temperature 50 to 75°C above the test temperature then cooled with no undercooling to the test temperature. This temperature history encourages cracking and minimises variation; this sequence represents T_4 to below T_6 in Fig. 1.1, rather than T_1 to T_3 in Fig. 1.1, where cracking can be difficult. After a short period at constant temperature, at least 30 minutes, the specimen was loaded to a K_I of about 15 MPa$\sqrt{m}$. The test history is depicted in Fig. 2.15. The value of K_I was calculated from Equation (2.1):

$$K_I = [P/(2t\sqrt{W})]f(a/W) \qquad (2.1)$$

where P = load (N);
t = wall thickness of the cladding (m);
W = effective width of specimen (m), being distance from the load line to the axis of rotation; see Fig. 2.13;
a = effective crack length (m), being distance from load line to the crack tip; see Fig. 2.13.

f (a/W) = geometry correction factor.

The value of f(a/W) was determined experimentally from compliance measurements, resulting in:

$$f(a/W) = 92.203 - 468.73(a/W) + 787.15(a/W)^2 - 360.99(a/W)^3 \qquad (2.2)$$

for LWR cladding [2.2] and

$$f(a/W) = -0.4759 + 13.185(a/W) + 39.533(a/W)^2 - 23.65(a/w)^3 + 12.135(a/W)^4 - 2.9162(a/W)^5 \qquad (2.3)$$

for CANDU cladding.

Cracking was detected either by potential drop (PD) or by displacement, equivalent to crack opening. Once the cracks had extended 2 to 3 mm, the load was removed and the specimen cooled to room temperature. The crack surfaces are lightly heat-tinted from oxidation and the ends of the crack can usually be discerned on the fracture surface. An alternative was to briefly fatigue the specimen to mark the end of the DHC. Subsequently, the specimen was broken open and the fracture surface examined. A typical pair of fracture surfaces is shown in Fig. 2.16. In this example the delayed hydride crack is about 3 mm long. Crack growth by DHC, a_F-a_0 (Fig. 2.16), was estimated on each crack from the average of nine equally spaced measurements; the value for the specimen, a_S, was the average of the values of the two cracks. Often an incubation period, t_i, was required before DHC started; cracking time, t_T, was taken as (time under load - t_i). Crack velocity, V, in the axial direction of the cladding was a_S/t_T. A scanning electron microscope (SEM) was used to examine the fracture surfaces of some specimens to provide details of the fracture mechanism.

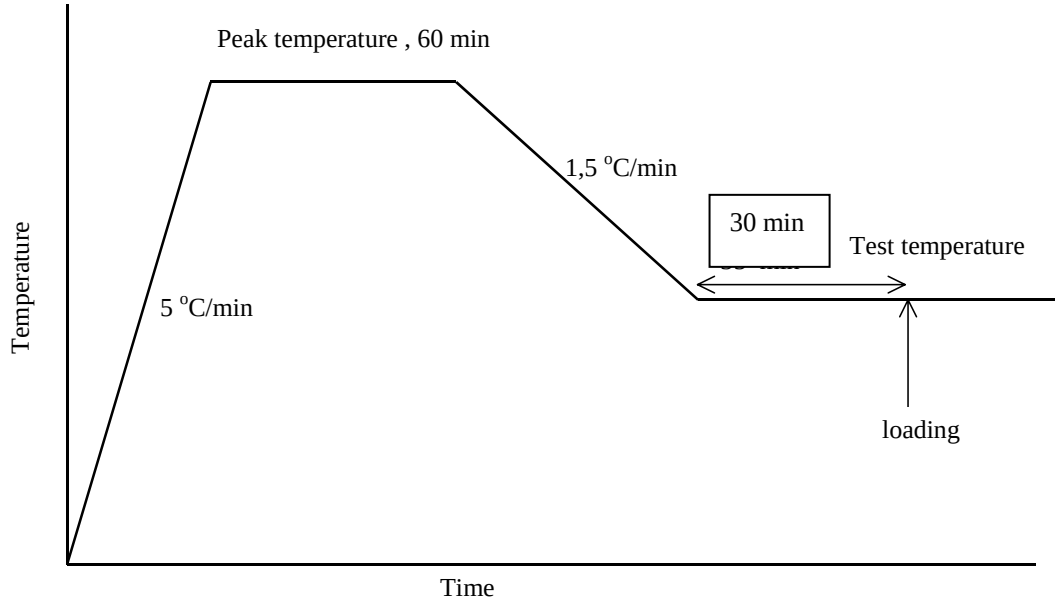

FIG. 2.15. Schematic diagram of the temperature cycle used for DHC tests.

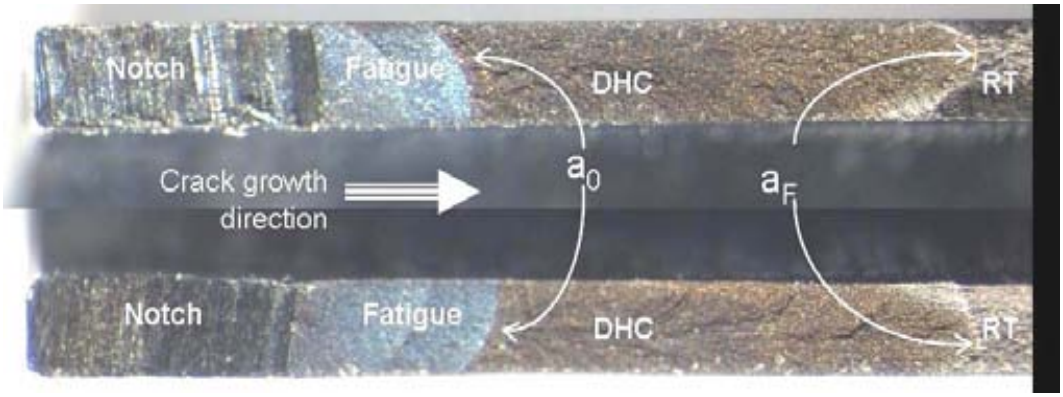

FIG. 2.16. View of the fracture surfaces of CWSR Zircaloy–4 specimen (200 ppm of hydrogen). The top and bottom edges are the outside surfaces of the cladding. The initial (a_0) and the final (a_F) length of the DHC crack are indicated as well as the areas of notch, fatigue pre-cracking, DHC crack propagation and room temperature fracture after the DHC test (RT).

A test matrix was established for phases 1 and 2 on the LWR material in which, in principle, each test temperature was sampled by at least two tests by three countries. Since it was quickly discovered that cracking was suppressed at high temperatures, the temperature intervals above 275ºC were much smaller than at lower temperatures. The nominal test matrix is given in Table 2.5. In practice, some temperatures were lightly sampled because of experimental difficulties.

TABLE 2.5. TEST MATRIX FOR DHC TESTING

Test temperature	Brazil, India, Lithuania			Argentina, Korea, Russia			Pakistan, Romania, Sweden		
ºC									
144	+								
186				+					
203	+								
227							+		
250	+			+			+		
283	+								
290				+					
295							+		
300				+					
310							+		

REFERENCES TO CHAPTER 2

[2.1] GRIGORIEV, V., JAKOBSSON, R., Application of the pin-loading tension test to measurements of delayed hydride cracking velocity in Zircaloy cladding, SKI Report 0057, Studsvik Nuclear AB, (November 2000).

[2.2] GRIGORIEV, V., JAKOBSSON, R., DHC axial crack velocity measurements in Zirconium alloy fuel cladding, STUDSVIK/N-05/281, Studsvik Nuclear AB, ISBN 91-7010-377-1, (December 2005).

CHAPTER 3

RESULTS

3.1. INITIAL TEST DATA

Typical test histories show the change in potential drop, Fig. 3.1(a), or displacement, Fig. 3.1(b), as a crack develops on loading after temperature cycling. If and when a crack propagates by DHC the period before cracking starts is indicated by no change in the values of PD or displacement. This incubation time is usually a small fraction of the whole test time and is highly variable.

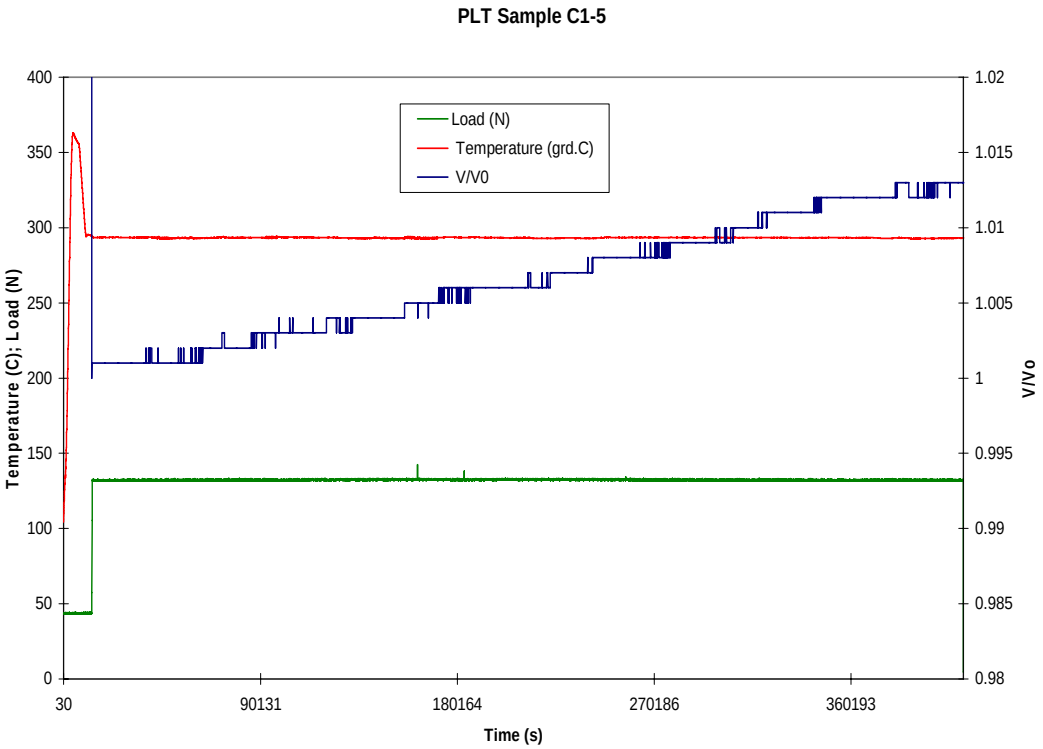

FIG. 3.1(a). Test history of specimen C1-5 (CANDU Zircatec Zircaloy tested at 295ºC) showing initial temperature cycle, loading and slow rise in potential drop after an incubation time of 66266 s.

3.2. PHASE 1: TESTS AT 250ºC ON PWR ZIRCALOY CLADDING (CWSR LOT 86080)

The details of each test are provided in appendix. The variation in incubation time is summarised in Table 3.1. The longest time before cracking was 16 200 s while in some tests cracking appeared to be instantaneous. The average of the mean values from each country was 4880 s. The standard deviation of the incubation time was 4628 s, emphasising the large scatter, which represents both variation in difficulty in initiating cracking and the ability to discern when cracking started.

TABLE 3.1. INCUBATION TIMES [s] OF ZIRCALOY–4 CLADDING (LOT 86080) AT 250ºC.

	Brazil	India	ROK	Lithuania	Pakistan	Romania	Russia	Sweden
	16200	600	3780	5340	303.6	0	8100	3720
	14400	2400	4260	10200	4140	0	1800	2580
	18000	3600	960	4200	3399	0	300	0
	10800	0	2700	8100	5022	0	4350	2760
		600	6120	2520	6175.2	0	210	720
		0	1500	4500	2276	1800		1800
		1800		2940	3780	0		
		1200		7320	9231	3420		
						2280		
						372		
						30		
						1200		
						4440		
Average	14850	1275	3220	5640	4291	1935*	2952	1930
Stdev	3074	1260	1905	2677	2660	1593*	3329	1380

* Values excluding zeros.

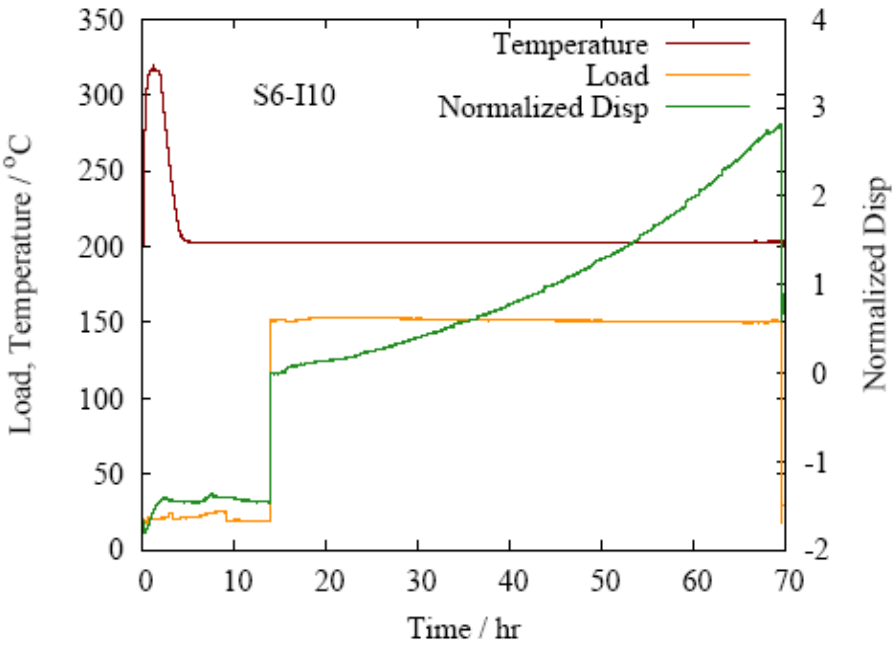

FIG. 3.1(b). Test history of specimen S6-I10 (Zircaloy from batch 86080 tested at 200ºC) showing initial temperature cycle, loading and gradual rise in crack-opening displacement after an incubation time of about 3600 s.

Crack velocity, V, was much more tractable, Table 3.2. The range of the mean value of each data set was from 2.42 to 3.97 × 10^{-8} m/s while the standard deviation ranged from 0.16 to 0.70 × 10^{-8} m/s; most values were about 0.3 × 10^{-8} m/s, representing about 11% variation. The maximum and minimum values in the whole data set were 4.72 × 10^{-8} m/s to 1.72 × 10^{-8} m/s, respectively. The mean value from all 64 specimens was 3.47 × 10^{-8} m/s with a standard deviation of 0.70 × 10^{-8} m/s. The peaked distribution of the values of V is shown in Fig. 3.2.

TABLE 3.2. DHC VELOCITIES [m/s×10^{-8}] OF ZIRCALOY–4 CLADDING (LOT 86080) AT 250ºC

	Argentina	Brazil	India	Korea	Lithuania	Pakistan	Romania	Russia	Sweden
	2.38	2.58	3.6	3.84	3.57	2.5	4.19	1.72	3.8
	2.52	2.15	2.76	3.61	3.28	3.4	3.6	2.55	3.9
	2.87	2.62	3.43	3.64	4.15	4.15	3.85	2.28	4.1
	2.25	2.2	3.7	3.92	3.31	4.72	3.89	3.03	3.7
	2.13		3.78	2.93	3.55	4.32	4.04	3.11	4
	2.34		3.91	3.56	3.78	3.32	4.36		4.1
			3.78		4.07	3.94	4.31		
			3.52		3.65	4.13	4.5		
							3.29		
							4.15		
							3.7		
							3.81		
							3.93		
Number of specimens	6	4	8	6	8	8	13	5	6
Mean V	2.42	2.39	3.56	3.58	3.67	3.81	3.97	2.54	3.93
Stdev V	0.26	0.25	0.36	0.35	0.32	0.70	0.34	0.57	0.16
Stdev/mean	0.11	0.10	0.10	0.10	0.09	0.18	0.08	0.23	0.04

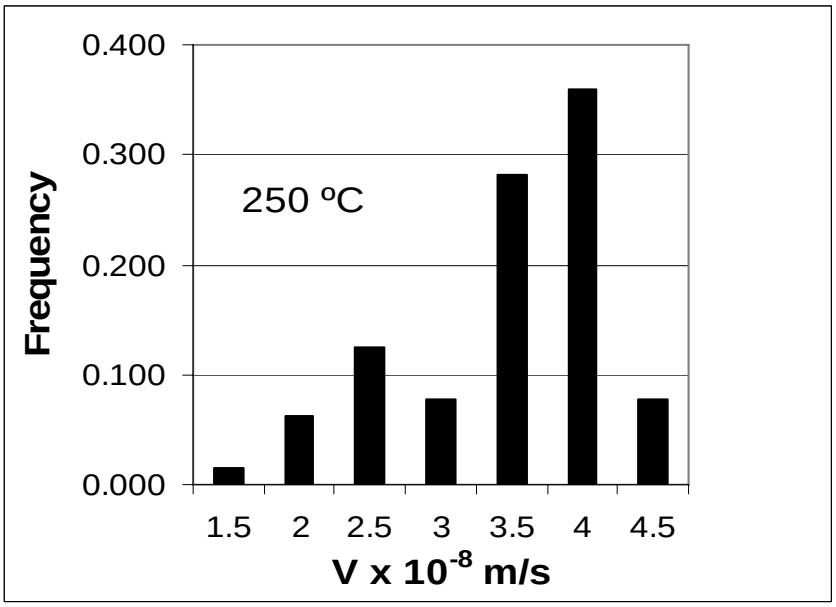

FIG. 3.2. Distribution of values of V in Zircaloy–4 from CWSR cladding from Lot 86080.

The possible causes of the scatter are metallurgical variations and experimental differences.

— The specimens and samples of fuel cladding came from the same lot and were randomized when sent to the various laboratories. Any metallurgical difference large enough to affect DHC through a difference in microstructure would be expected to be picked up during the fabrication and inspection of the tubing. No such difference was reported so microstructural variation is not contributing to the scatter. Later results will support this conclusion.

— Small variations in temperature history may affect the values of V. Great care was taken to avoid under-cooling when attaining the test temperature and the cooling rate in all the laboratories was similar being 1 to 3ºC/min. In some laboratories the test temperatures had a small deviation from the target temperature and this factor may have contributed a small deviation, Fig. 3.3, although other factors are clearly contributing to the scatter. The line marked 'whole population' represents the temperature dependence based on Equation 1.1, to be described in Section 3.3.

— A small variation in the peak temperature could contribute to the scatter. The total hydrogen concentration was 200 ppm so not all the hydrogen was taken into solution during heating to the peak temperature — the temperature would have to be taken to about 400ºC to dissolve all the hydrogen [3.xxix]. With small variations in the peak temperature, differences in the amount of hydrogen in solution at the test temperature would exist. In the small range of differences in peak temperature it is difficult to discern more than a suggestion of an effect, Fig. 3.4.

— Some laboratories had difficulties with preparing the initial crack by fatigue. If the final value of maximum K_I during fatigue is smaller than the K_I applied during the DHC test, the latter cracking should be well behaved. Any upper deviation from this target during fatigue would mostly affect the initiation times rather than V. A typical successful fatigue sequence is described in Chapter 2.

— The wide variation in incubation time could contribute to the scatter to V if t_i is in error. The total time of a test is very accurately known because it corresponds to the time of unloading the specimen. The average cracking time was 6.87×10^4 s ± 2.55×10^4 s and the average incubation time and the incubation time in individual tests was about 6% of the cracking time. The contribution of the scatter in incubation time to the variation of V was therefore small.

— The initial value of K_I depends on the load and the crack length after fatigue. The load is well known but the initial crack length has some variation because it is difficult to measure accurately. For these tests the target for the initial value of K_I was 15 MPa√m. In practice it varied between 11 and 22.8 MPa√m, but the mean value was 15.1 MPa√m, close to the target, with a moderate dispersion of 2.0 MPa√m. Most laboratories obtained seemingly valid results with amounts of crack growth varying from 1.5 mm to 4.2 mm; the mean value for all the tests at 250ºC was 2.4 ± 0.6 mm. Consequently the final value of K_I had a wide range, from 21.1 MPa√m to 38.9 MPa√m, with a mean value of 26.8 ± 3.5 MPa√m. One expects that V should be independent of either initial or final K_I (so long as K_{IH} is exceeded) and therefore crack length, and the results confirm this expectation, with some slight negative dependence with very low correlations, Fig. 3.5 and Fig. 3.6.

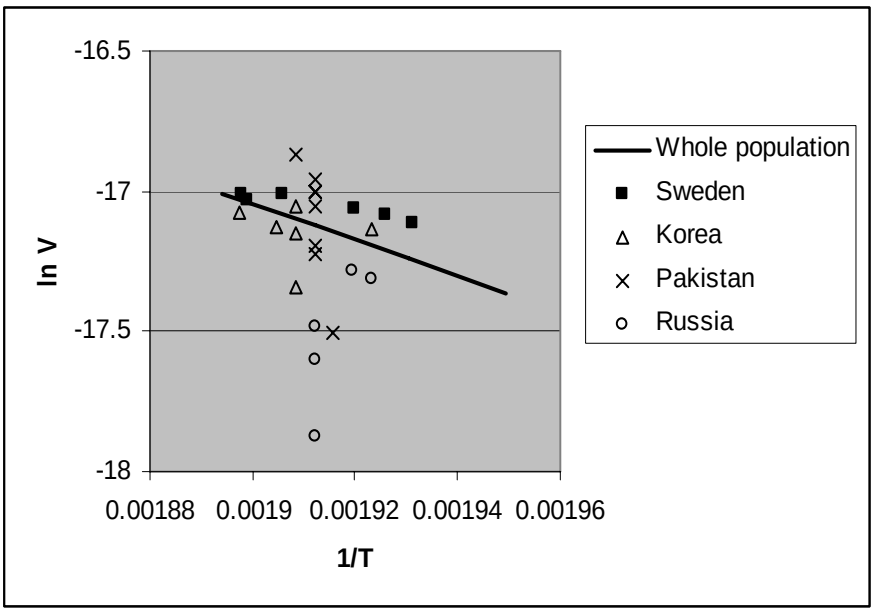

FIG. 3.3. Scatter in V partly as a consequence of deviation from 250ºC.

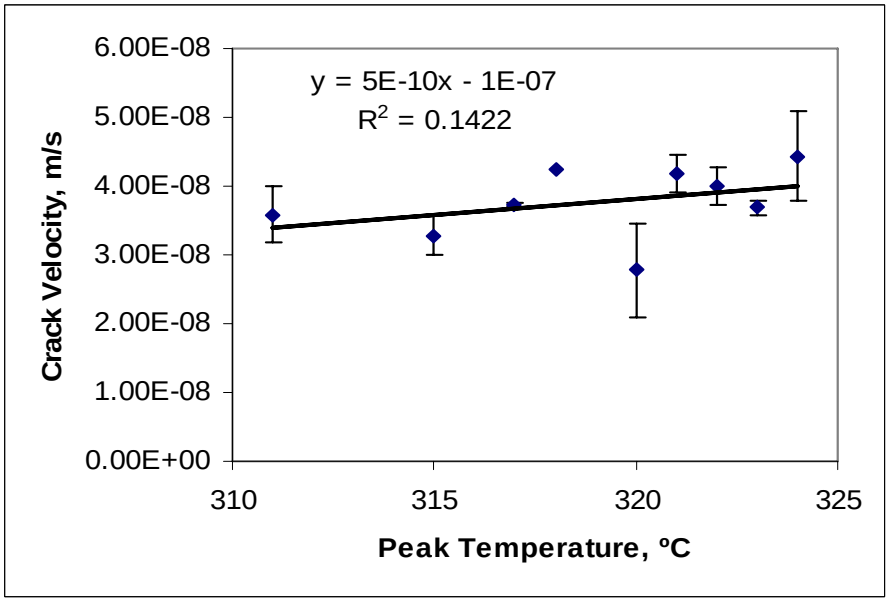

FIG. 3.4. Effect of peak temperature on V at 250ºC in CWSR Zircaloy–4 fuel cladding.

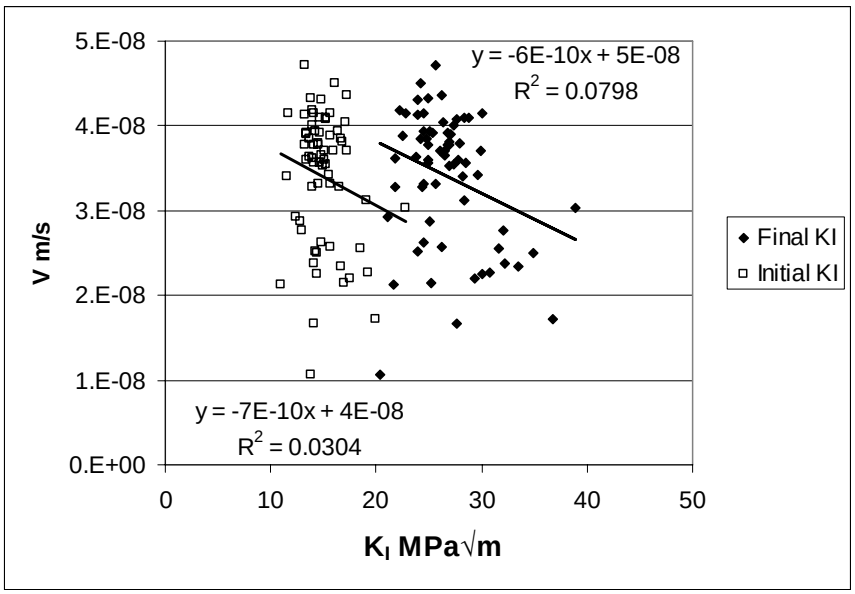

FIG. 3.5. Independence on either initial or final K_I of V at 250ºC for CWSR Zircaloy–4 fuel cladding.

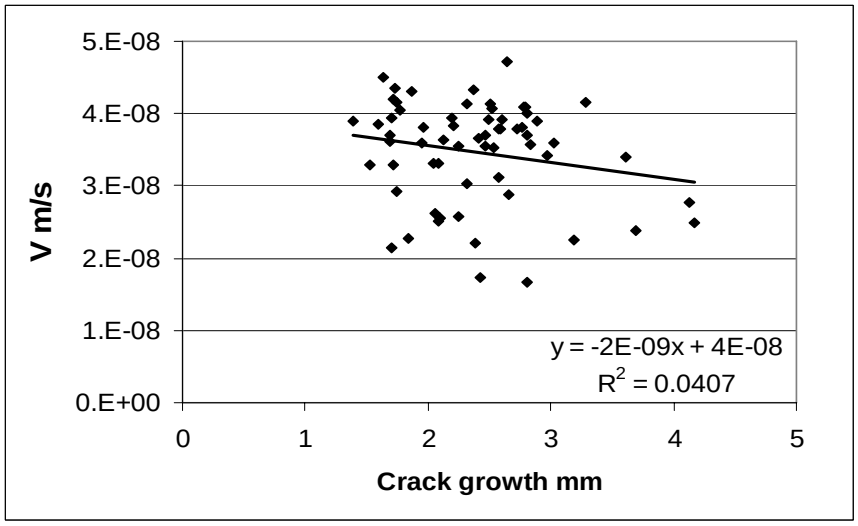

FIG. 3.6. Lack of dependence or correlation between amount of crack growth and V at 250ºC for CWSR Zircaloy–4 fuel cladding.

Temperature control appears to be the most important factor contributing to the scatter in the data; the remaining factors were under control and the data are considered satisfactory and represent the DHC behaviour of CWSR fuel cladding at 250ºC. The same testing technique was then applied at several temperatures above and below 250ºC.

3.3. PHASE 1: TESTS AT TEMPERATURES OTHER THAN 250ºC ON PWR ZIRCALOY CLADDING (CWSR LOT 86080)

The details of each test are provided in the Appendix. At temperatures above about 275ºC cracking was found to be very difficult and often there was no cracking. The results will be presented with this phenomenon as background.

Up to 275ºC the variation in incubation time is summarised in Table 3.3 and plotted in Fig. 3.7. The data are very scattered and, although the expected decline in t_i with increase in test temperature is indicated, the correlation is very poor. Results from higher test temperatures were very variable and depended on how long the experimenter was prepared to wait without any sign of cracking; some specimens were loaded for times over 100 000 s (greater than one day) at temperatures where one would expect times to be ten times smaller.

The crack velocities between 150 and 300ºC (excluding those at 250ºC) are summarised in Table 3.4. Although the number of specimens tested was small, the standard deviations of the mean values were less than 15% while the range of values at any one temperature was less than a factor of 1.5. Below 275ºC the values of crack velocity have a clear and highly correlated temperature dependence following Equation 1.1. Fig. 3.8 represents the mean values including the data from tests at 250ºC. Q has a value of 53.1 kJ/mol. Above 275ºC the cracking was very variable with a tendency to decline from the values expected by an extrapolation of Equation 1, as indicated in Fig. 3.9.

TABLE 3.3. INCUBATION TIMES BEFORE DHC STARTED IN ZIRCALOY–4 CLADDING (LOT 86080) AT TEST TEMPERATURES UP TO 275ºC

Temperature,ºC.	150	185	200	227	250	275
Mean value, s	44 660	88 500	5730	11 580	4880	28 366
Standard deviation, s	39 100	69 298	10 072	6206	4630	34 622
Maximum value, s	72720	15 3180	20 820	17 388	16 200	61 680
Minimum value, s	0	15360	0	5040	0	6300

TABLE 3.4. SUMMARY OF CRACK VELOCITIES IN ZIRCALOY–4 CWSR LOT 86080

Test temperatureºC	150	185	200	227	232	275	280	283	290	300
Crack velocity	0.21	0.53	0.85	2.56	2.7	6.11	8.4	0*	0	0.55
10^{-8} m/s	0.20	0.63	0.79	2.3		5.75	3.65	4.66		0
	0.23	0.64	0.89	1.93		4.82	0			0
			0.97			6.58				
						6.64				
						6.89				
Mean value	0.21	0.60	0.87	2.26	2.70	6.13				
Standard deviation	0.012	0.064	0.077	0.317	…	0.762				
Stdev/mean	0.058	0.106	0.088	0.140	…	0.124				
Highest V/lowest V	1.12	1.22	1.23	1.33	…	1.43				

* Values plotted as (0.001 mm/test time)

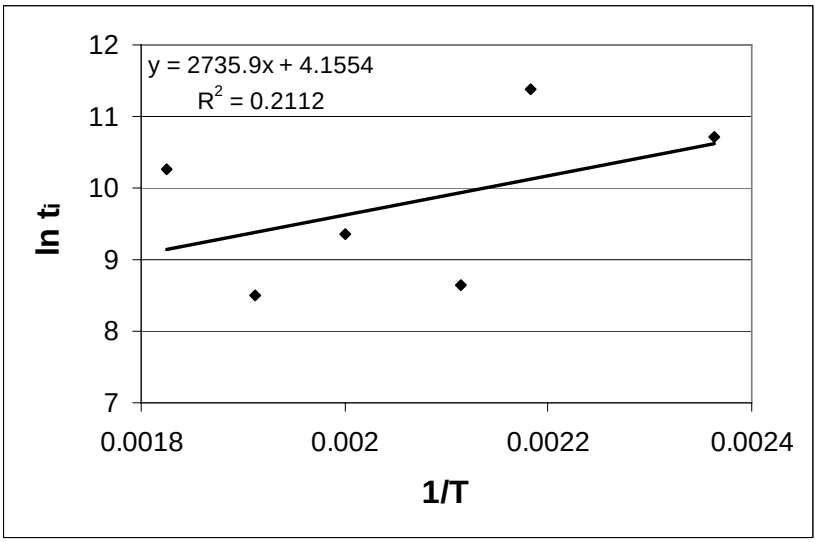

FIG. 3.7. Temperature dependence of mean incubation time for DHC in CWSR Zircaloy–4 cladding from Lot 86080.

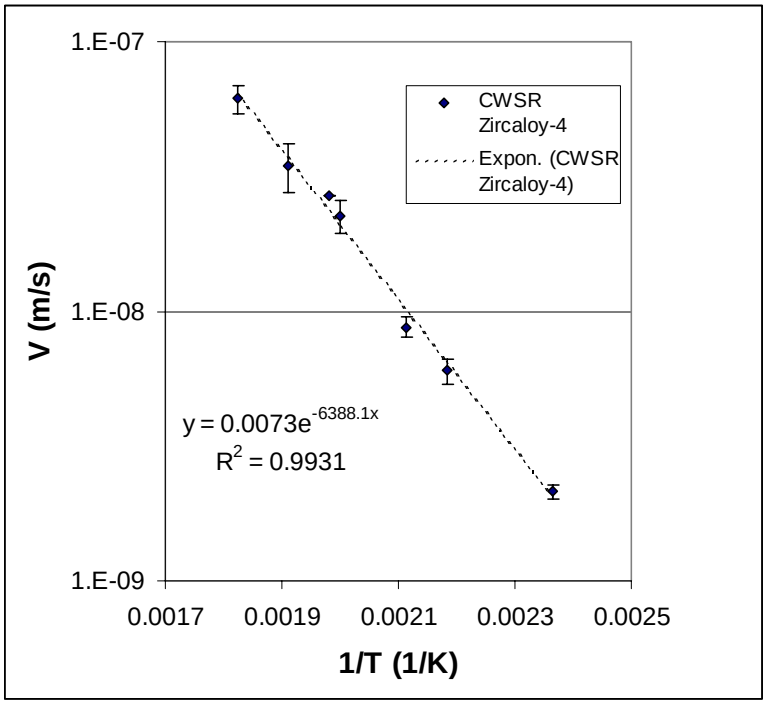

FIG. 3.8. Temperature dependence of crack velocity between 150 and 273ºC in CWSR Zircaloy–4 cladding from Lot 86080: mean values.

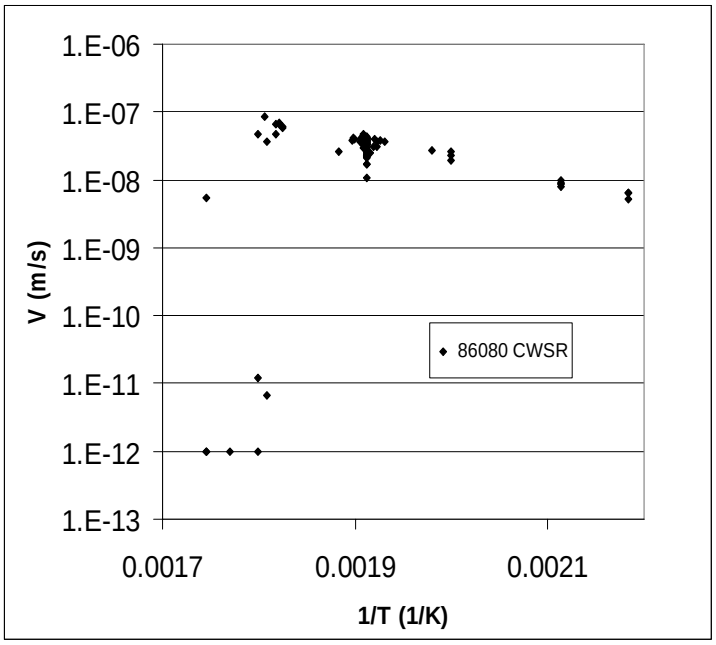

FIG. 3.9. Temperature dependence of crack velocity between 150 and 300ºC in CWSR Zircaloy–4 cladding from Lot 86080 showing sudden decline in cracking above 275ºC — all data.

3.4. PHASE 2: TESTS AT VARIOUS TEMPERATURES ON LWR ZIRCALOY CLADDING (LOT 83786).

Three sets of experiments were done on this fuel cladding: DHC was measured in the same temperature range as in Phase 2 on the material in the cold worked condition and after two heat-treatments that represented the metallurgical condition for the fuel cladding for PWR (480ºC for 3.5 h) and BWR (565ºC for 1.5 h).

3.4.1 Testing of material in the cold worked condition

The details of each test are provided in the Appendix. As with the tests on Lot 86080, the incubation time was very scattered and showed very little temperature dependence, Fig. 3.10. The mean initial value of K_I was 16.5±2.9 MPa√m and the average crack growth in all the tests was 1.73±0.91 mm providing a final value of K_I of 25.2±6.1 MPa√m. The values of V showed strong and clear temperature dependence. As in Phase 1, the data followed Equation 1.1 up to about 275ºC then exhibited a sudden decline. The data are summarised in Table 3.5 and plotted in Fig. 3.11 up to 275ºC then up to 300ºC in Fig. 3.12. From Fig. 3.11, Q is estimated to be 54.8 kJ/mol.

TABLE 3.5. SUMMARY OF CRACK VELOCITIES IN ZIRCALOY–4 LOT 83786 IN THE COLD WORKED CONDITION

Test temperature	144	150	185	200	225	231	250	275	285	290	295	300
ºC												
Crack velocity	0.2	0.26	0.9	2	3.54	4.3	6.26	7.2	8.64	8.17	0.2	0.24
10^{-8} m/s	0.2		0.9	1.24	3.43		6.07				0.94	3.08
	0.21			1.29			5.72				0.024	4.69
				1.2			6.9					3.96
							4.1					0.0058*
							4.6					0.0058*
							3.6					
							4.6					
Mean value	0.203	0.26	0.89	1.43	3.49	4.3	5.23	7.2	8.64	8.17	0.39	
Standard deviation	0.006	…	…	0.38	…	…	1.17	…	…	…	…	

* Values taken as (0.001/test time)

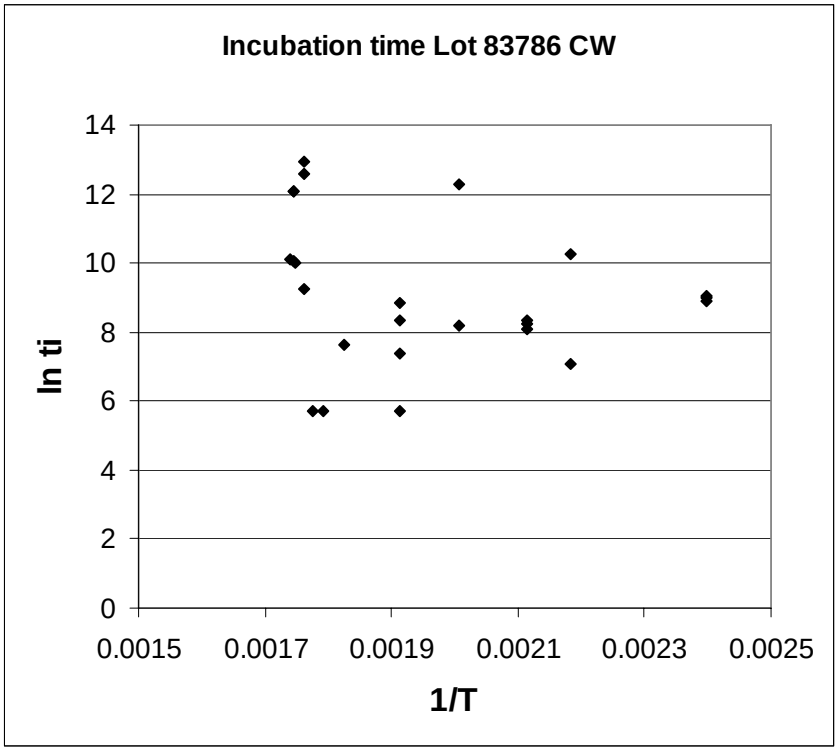

FIG. 3.10. Effect of temperature on time to initiate cracks in Zircaloy–4 cladding from Lot 83786 in the cold worked condition.

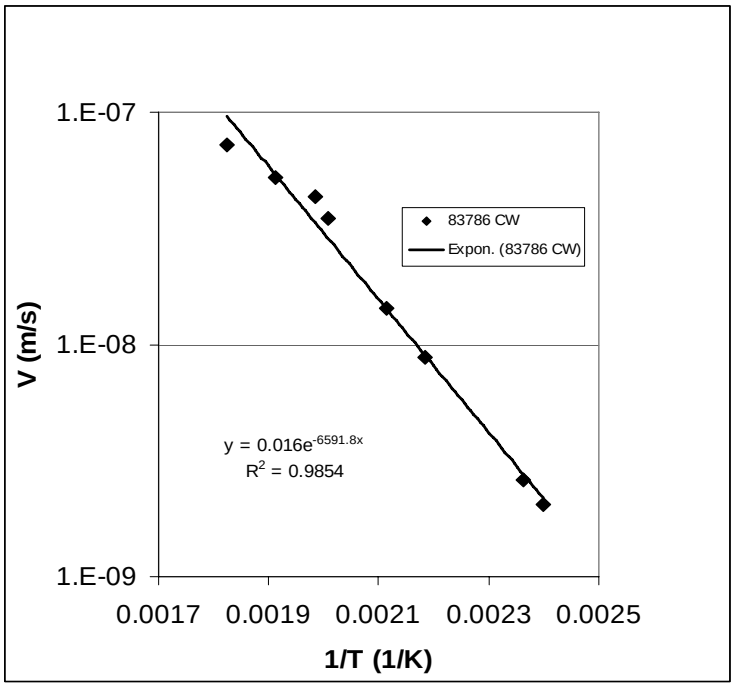

FIG. 3.11. Temperature dependence of crack velocity between 150 and 273ºC in CW Zircaloy–4 cladding from Lot 83786: mean values.

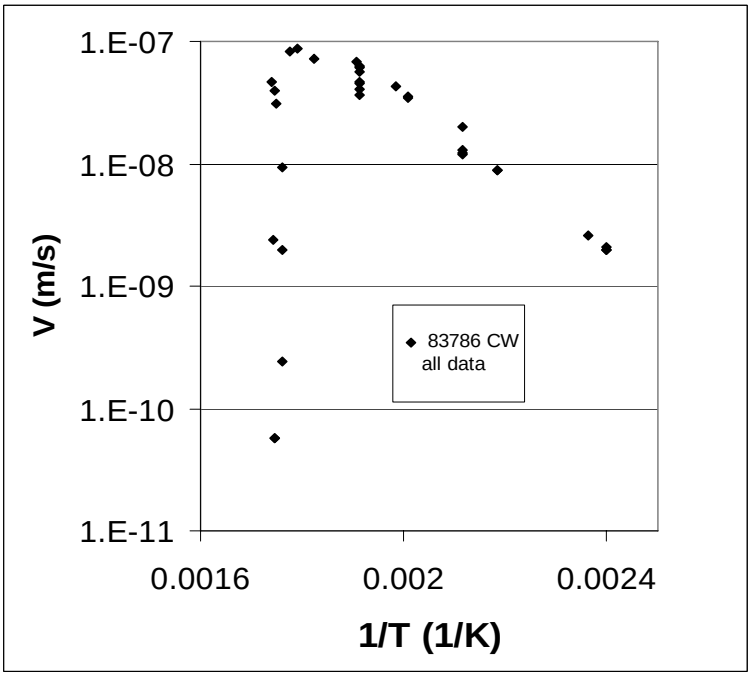

FIG. 3.12. Temperature dependence of crack velocity between 150 and 300ºC in CW Zircaloy–4 cladding from Lot 83786 showing sudden decline in cracking above 275ºC – all data.

3.4.2. Testing of material in the cold worked and stress relieved condition (480ºC for 3.5 h)

The details of each test are provided in the Appendix. As with the tests on Lot 86080 and the cold worked material, the incubation time was very scattered and showed very little temperature dependence, Fig. 3.13. The mean initial value of K_I was 17.3±4.1 MPa√m and the average crack growth in all the tests was 1.42±0.94 mm providing a final value of K_I of 24.8±7.3 MPa√m. Similarly the values of V showed a strong and clear temperature dependence with the data followed Equation 1.1 up to about 275ºC then exhibited a sudden decline. The data are summarised in Table 3.6 and plotted in Fig. 3.14 up to 275ºC then up to 300ºC in Fig. 3.15. From Fig. 3.14, Q is estimated to be 54.9 kJ/mol.

TABLE 3.6. SUMMARY OF CRACK VELOCITIES IN ZIRCALOY–4 LOT 83786 IN THE COLD WORKED AND STRESS RELIEVED-CONDITION

Temperature	144	185	200	215	225	250	275	279	282	283	290	295
C												
Crack velocity	0.12	1.11	0.96	1.37	2.27	4.24	5.31	2.29	12.3	0.11	6.17	0.41
10-8 m/s	0.124	1.15	1.07		2.79	3.8		3.45	8.78	0.12		0.17
	0.010	0.375	0.87			3.12		4.35	0.81			0.01
	0.127	0.459	1.07			2.44			0.50			
	0.1											
Mean value	0.118*	0.77	0.99	1.37	2.53	3.4	5.31	3.36	5.6	0.12	6.17	0.198
Standard deviation	0.012	0.41	0.10	…	…	0.79	…	1.03	2.49	0.004	…	0.202

*Lowest value excluded.

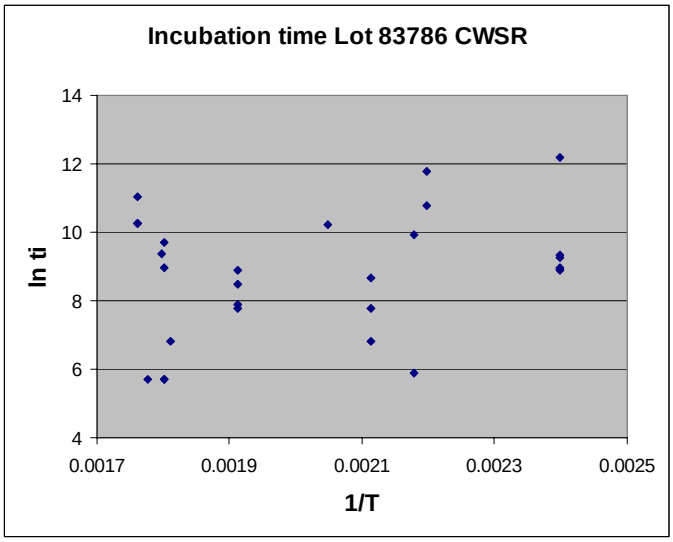

FIG. 3.13. Effect of temperature on time to initiate cracks in Zircaloy–4 cladding from Lot 83786 in the cold worked stress relieved condition. All data.

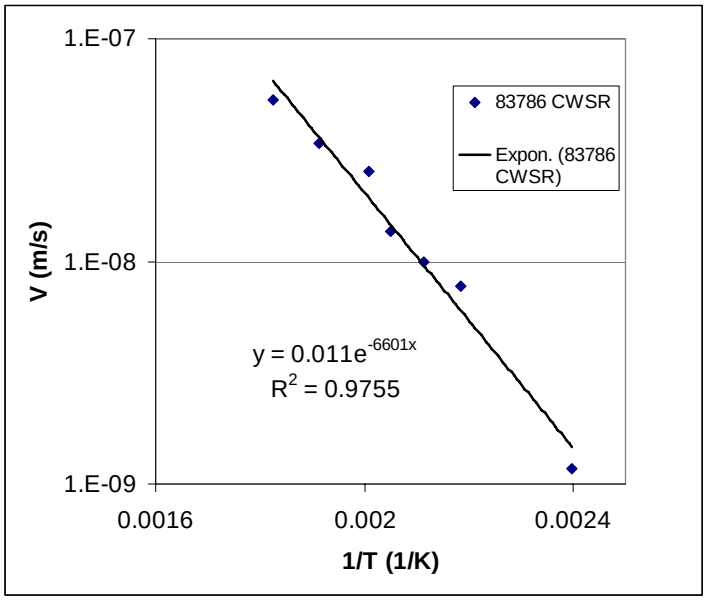

FIG. 3.14. Temperature dependence of crack velocity between 150 and 273ºC in CWSR Zircaloy–4 cladding from Lot 83786 – mean or single values.

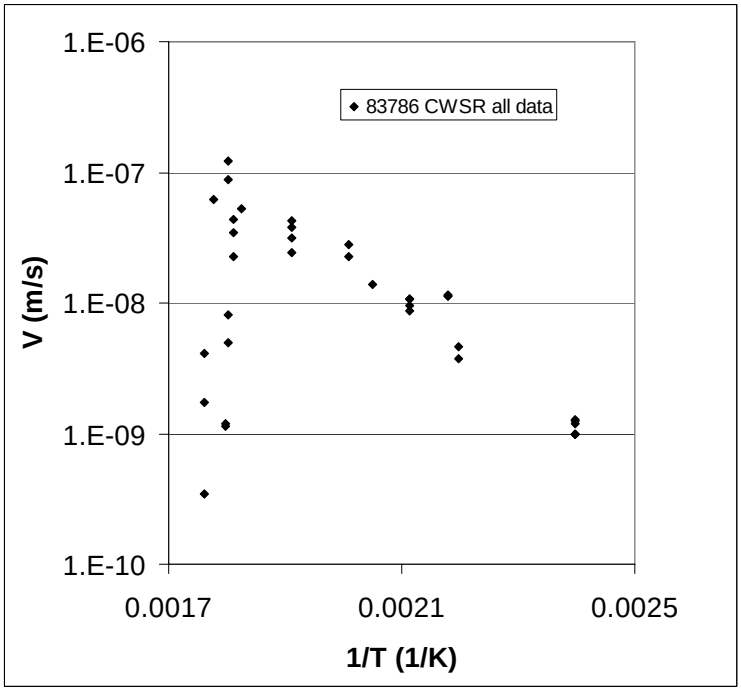

FIG. 3.15. Temperature dependence of crack velocity between 150 and 300ºC in CWSR Zircaloy–4 cladding from Lot 83786 showing sudden decline in cracking above 275ºC – all data.

3.4.3. Testing of material in the recrystallized condition (565ºC for 1.5 h).

The details of each test are provided in the Appendix. The DHC behaviour of this material was extremely variable. The incubation time was very scattered and showed very little temperature dependence, Fig. 3.16. The mean initial value of K_I was 17.6±3.2 MPa$\sqrt{m}$. The values of V were also very variable and exhibited little temperature dependence. The data are summarised in Table 3.7 and plotted in Fig. 3.17.

TABLE 3.7. SUMMARY OF CRACK VELOCITIES IN ZIRCALOY–4 LOT 83786 IN THE RECRYSTALLISED CONDITION

Test temperature	144	182	200	225	250	282	295
ºC							
Crack velocity	3.1E-13	2E-12	7.89E-11	2.79E-09	1.83E-12	6.8E-09	1.16E-13
m/s	3.5E-11	6.97E-14	7.6E-10	3.36E-09	1.94E-12		2.87E-11
			7.4E-09		7.8E-10		3.14E-14
			5.2E-10		5.91E-13		
			8.1E-09		3.60E-08		
					1.50E-08		
					1.1E-09		

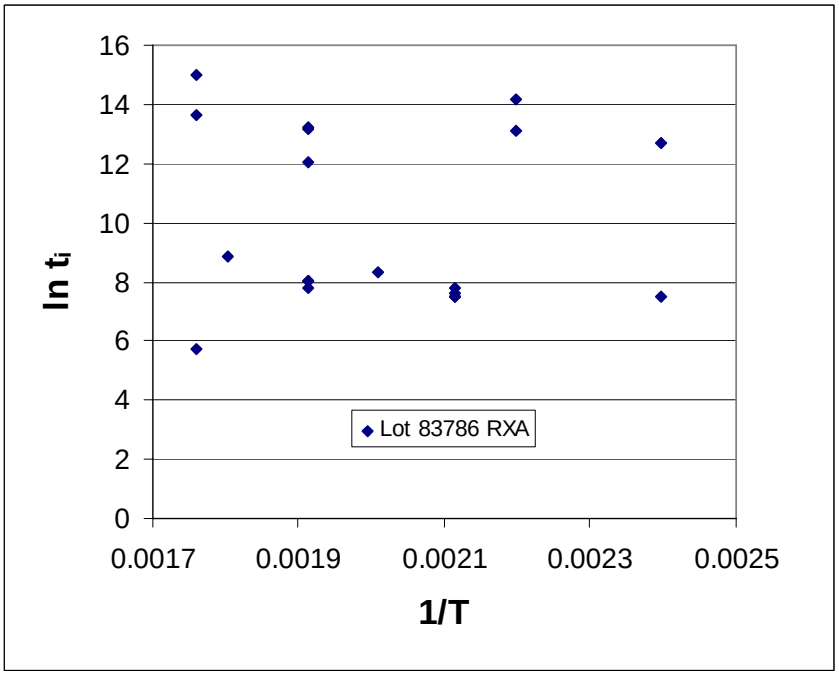

FIG. 3.16. Effect of temperature on time to initiate cracks in Zircaloy–4 cladding from Lot 83786 in the recrystallized condition — all data.

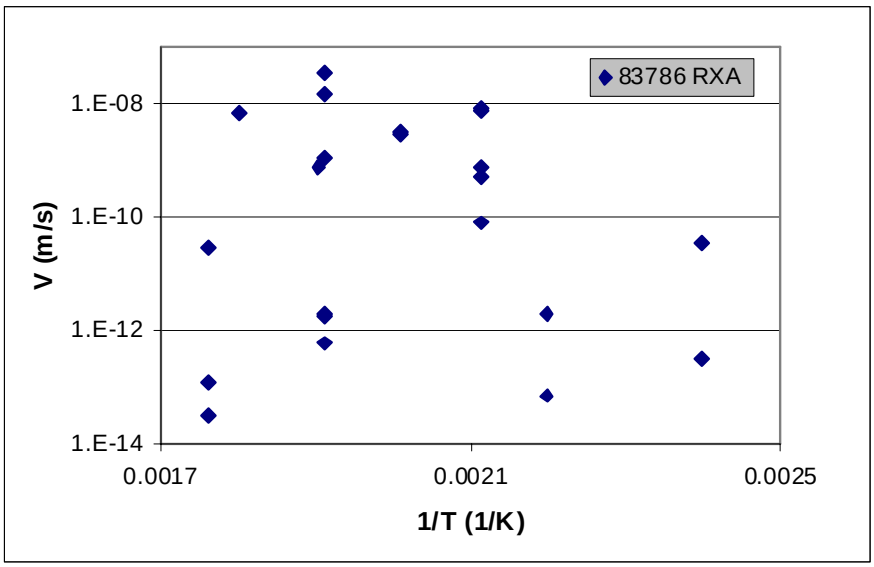

FIG. 3.17. Temperature dependence of crack velocity in recrystallized Zircaloy–4 cladding from Lot 83786 — all data.

3.5. PHASE 3: TESTS AT VARIOUS TEMPERATURES ON ATUCHA AND CANDU CLADDING.

The details of each test are provided in the Appendix. Since only a few tests have been completed on these materials, it is difficult to make more than general observations. The velocity data are summarised in Table 3.8 for each material.

TABLE 3.8. SUMMARY OF CRACK VELOCITIES IN ZIRCALOY–4 TYPICAL OF ATUCHA AND CANDU MATERIAL FROM ZIRCATEC AND SANDVIK

Atucha	Test Temperature		200	225	250	295
	ºC					
	Crack velocity		1.78E-09	2.84E-09	4.76E-09	3.96E-10
	m/s		2.18E-09	2.50E-09	4.28E-09	3.14E-10
					5.30E-09	
					4.46E-09	
					3.10E-09	
					2.08E-09	
		mean	1.98E-09	2.67E-09	4.00E-09	3.55E-10
CANDU				2.77E-09	5.98E-09	4.32E-10
Zircatec				2.41E-09	5.82E-09	9.95E-10
		mean		2.59E-09	5.90E-09	7.14E-10
CANDU					2.45E-08	
Sandvik					2.67E-08	
					3.25E-08	
					3.92E-08	
					2.53E-08	
		mean			2.96E-08	

3.5.1. Atucha

The incubation times were very scattered and showed no temperature dependence, Fig. 3.18. The mean initial value of K_I was 15.5±1.5 MPa√m. Between 200 and 250ºC, V increased in the expected manner, although was somewhat scattered, but the values at 295ºC were low, in line with the earlier data. The estimate of Q is unreliable because of the paucity of data. Four methods were used: pooling the data between 200 and 250ºC, with and without the lowest value at 250ºC, and using the mean value at each temperature, again with and without the lowest value at 250ºC. The values are:

	Q [kJ/mol]
All data	27.7
All data (without lowest value at 250ºC)	33.1
Mean values	28.9
Mean values (without lowest value at 250ºC)	32.5

This exercise demonstrated the sensitivity of Q to individual points when the temperature range is small.

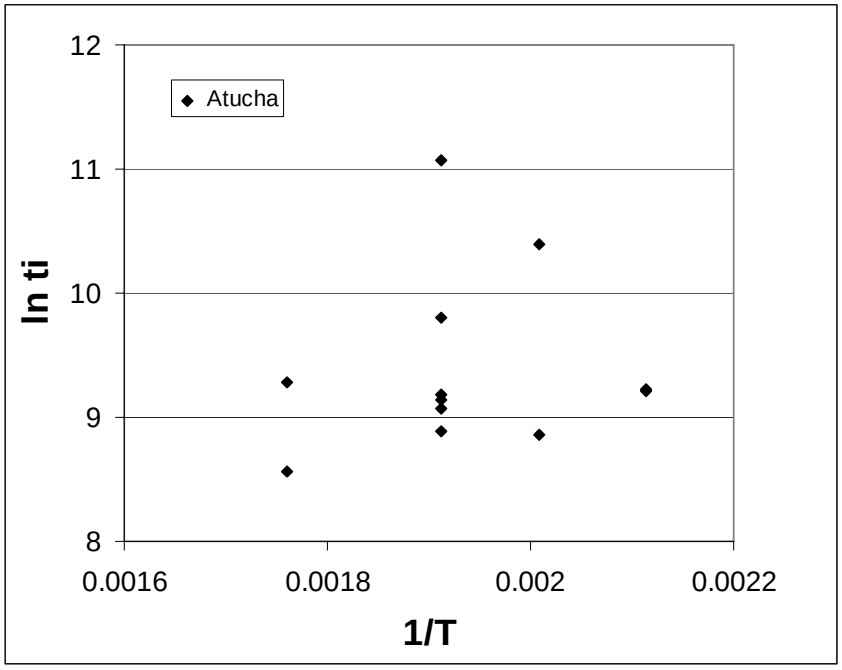

FIG. 3.18. Effect of temperature on time to initiate cracks in Atucha Zircaloy–4 cladding.

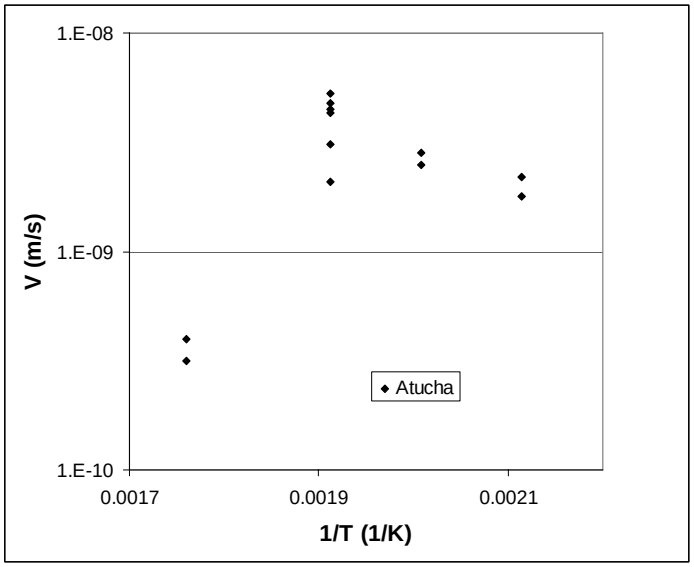

FIG. 3.19. Temperature dependence of crack velocity in Atucha Zircaloy–4 cladding — all data.

3.5.2. CANDU Zircatec

The incubation times were scattered and showed no temperature dependence, Fig. 3.20. The mean initial value of K_I was 16.3±0.5 MPa√m. Between 225 and 250ºC, V increased in the expected manner but the values at 295ºC were low, in line with the earlier data, Fig. 3.21. Again the estimate of Q is unreliable because tests were done at only two temperatures; a value of 71.4 kJ/mol was obtained but should be used with caution.

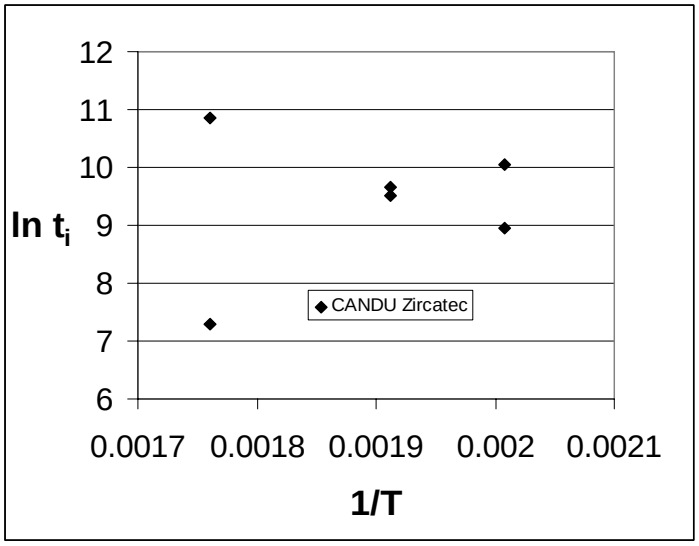

FIG. 3.20. Effect of temperature on time to initiate cracks in CANDU Zircaloy–4 cladding from Zircatec.

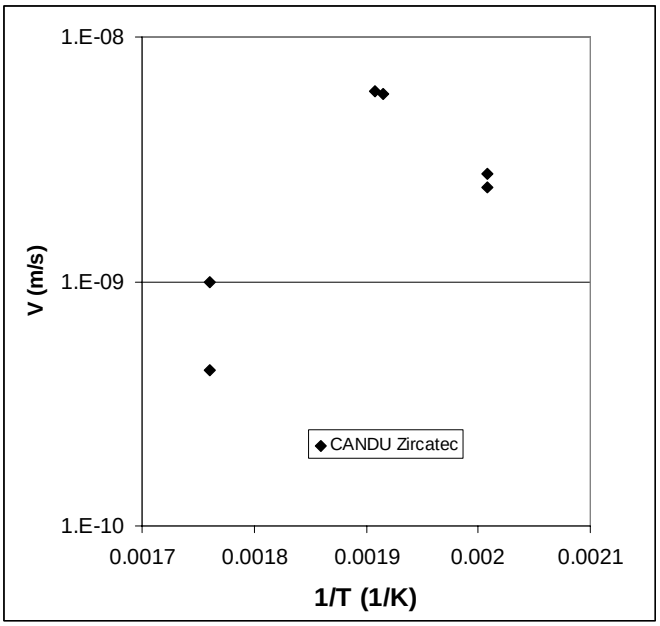

FIG. 3.21. Temperature dependence of crack velocity in CANDU Zircaloy–4 cladding from Zircatec — all data.

3.5.3. CANDU Sandvik

This material was tested at one temperature, 250ºC. The mean initial value of K_I was 17.3±1.4 MPa√m. The mean value of V was 2.96×10^{-8} m/s with a standard deviation of 6.2×10^{-9} m/s.

3.6. FRACTOGRAPHY

Some specimens have been examined in the scanning electron microscope (SEM). The three parts of the fracture surface, namely fatigue precracking, DHC and post-test rupture, can be distinguished and changes in fracture mode can be clearly delineated. Examples from tests at 250ºC on CANDU materials are given in Figs. 3.22 to 3.25. Fig. 3.22 illustrates the striations associated with the fatigue pre-cracking. Note that these striations are formed at room temperature and have been oxidized during DHC testing. Fig. 3.23 depicts ductile fracture at 250ºC after DHC is completed; the large fissures between the areas of ductile dimples are probably fractured hydrides that are perpendicular to the fracture plane. DHC is shown in Fig. 3.24 as areas of flat fracture interspersed by curved features that correspond to changes in crack plane or direction. The interface between fatigue and DHC is portrayed in Fig. 3.25. Fractographs of the materials in other metallurgical states showed the same features. To date, striations have been observed only once, Fig. 3.26. This specimen was CWSR Zircaloy–4 cladding and the striations were in the high K_I region, between about 25 to 40 MPa√m. This specimen had been subjected to 12 temperature cycles between 248 and 270ºC.

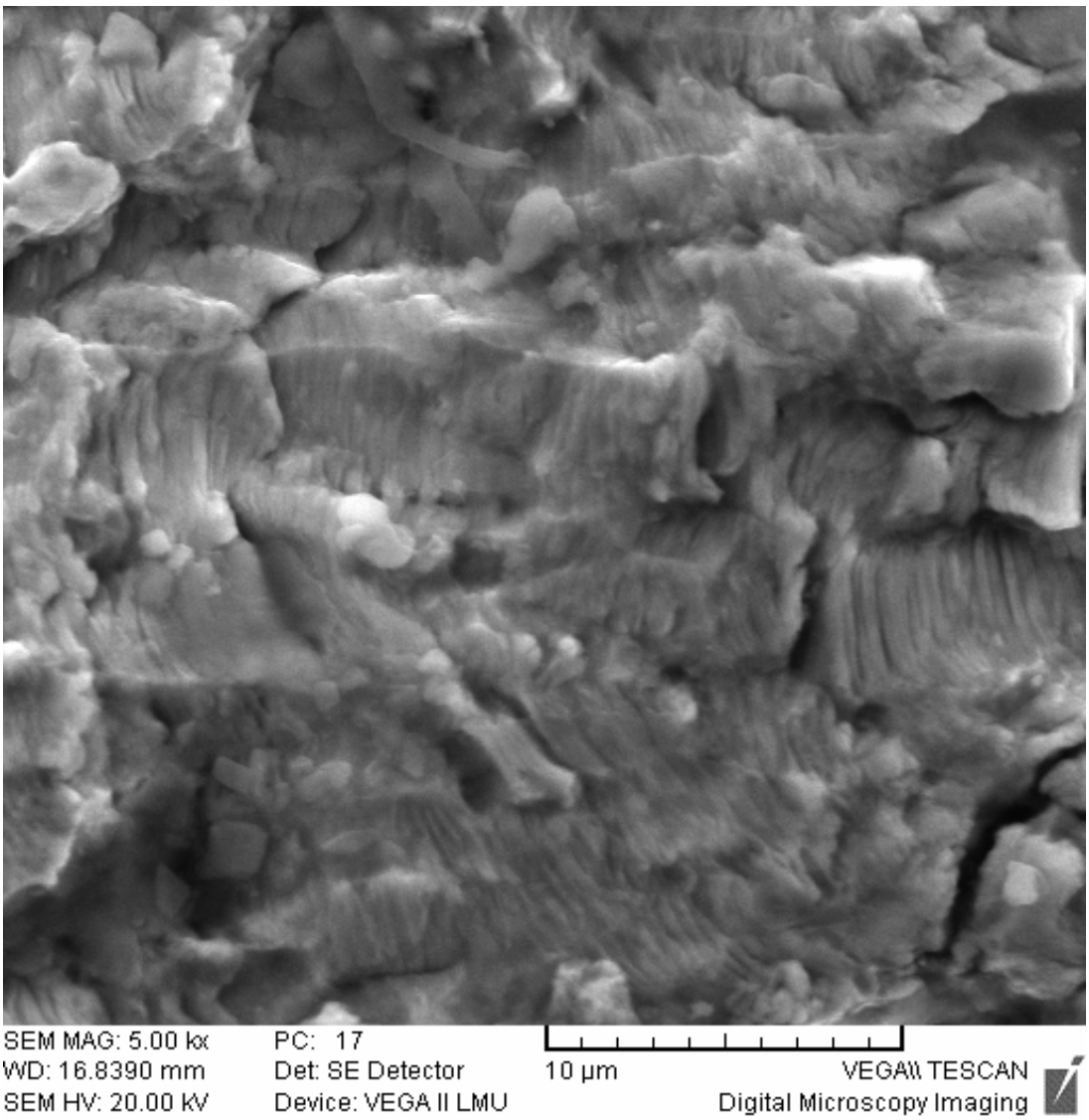

FIG. 3.22. Fatigue striations formed at room temperature on Specimen C1-1; CANDU Zircaloy tested at 250ºC.

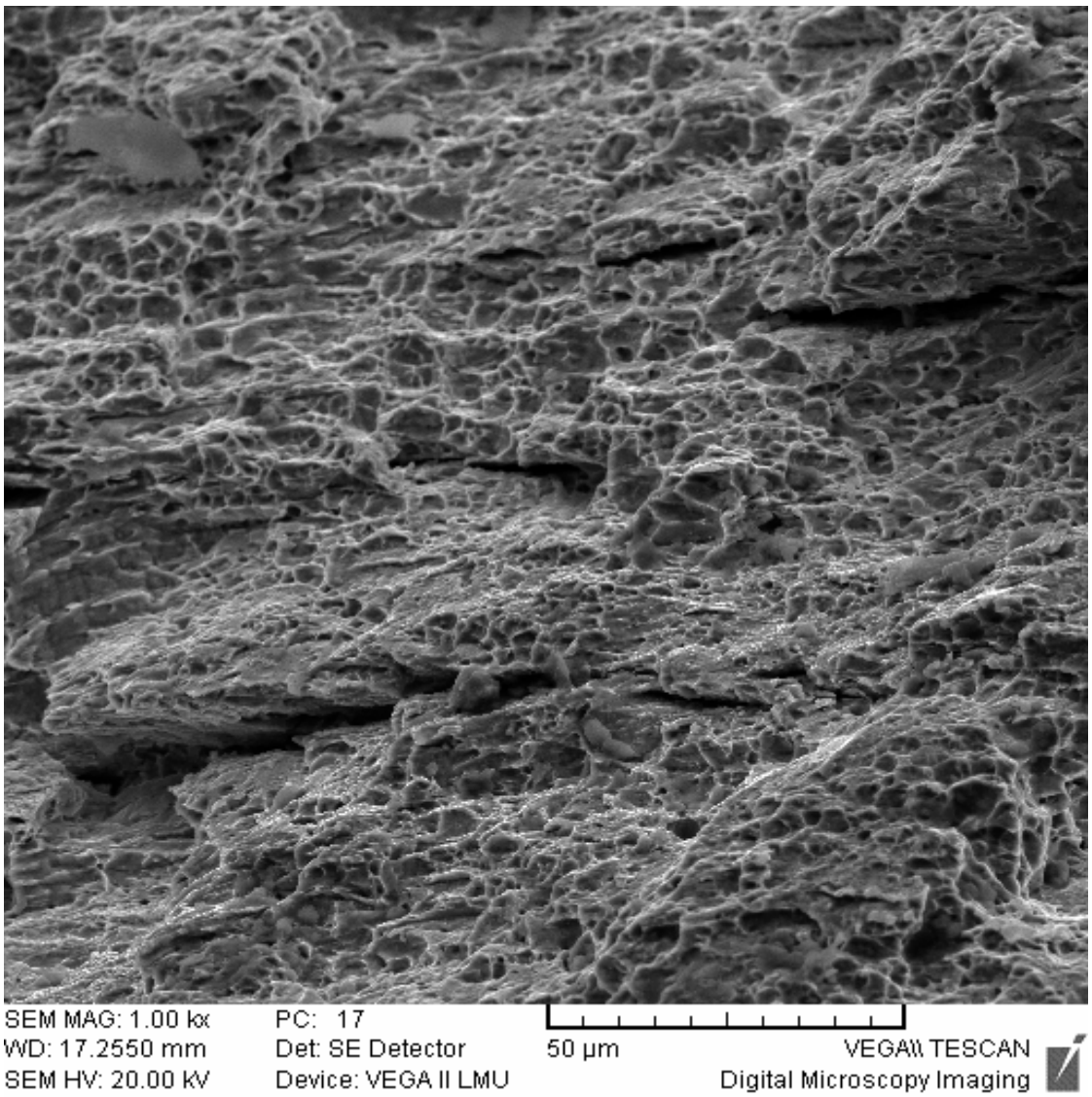

FIG. 3.23. Ductile dimples on specimen C1-1 formed at 25ºC after DHC test; CANDU Zircaloy–4 tested at 250ºC. Cracking from right to left.

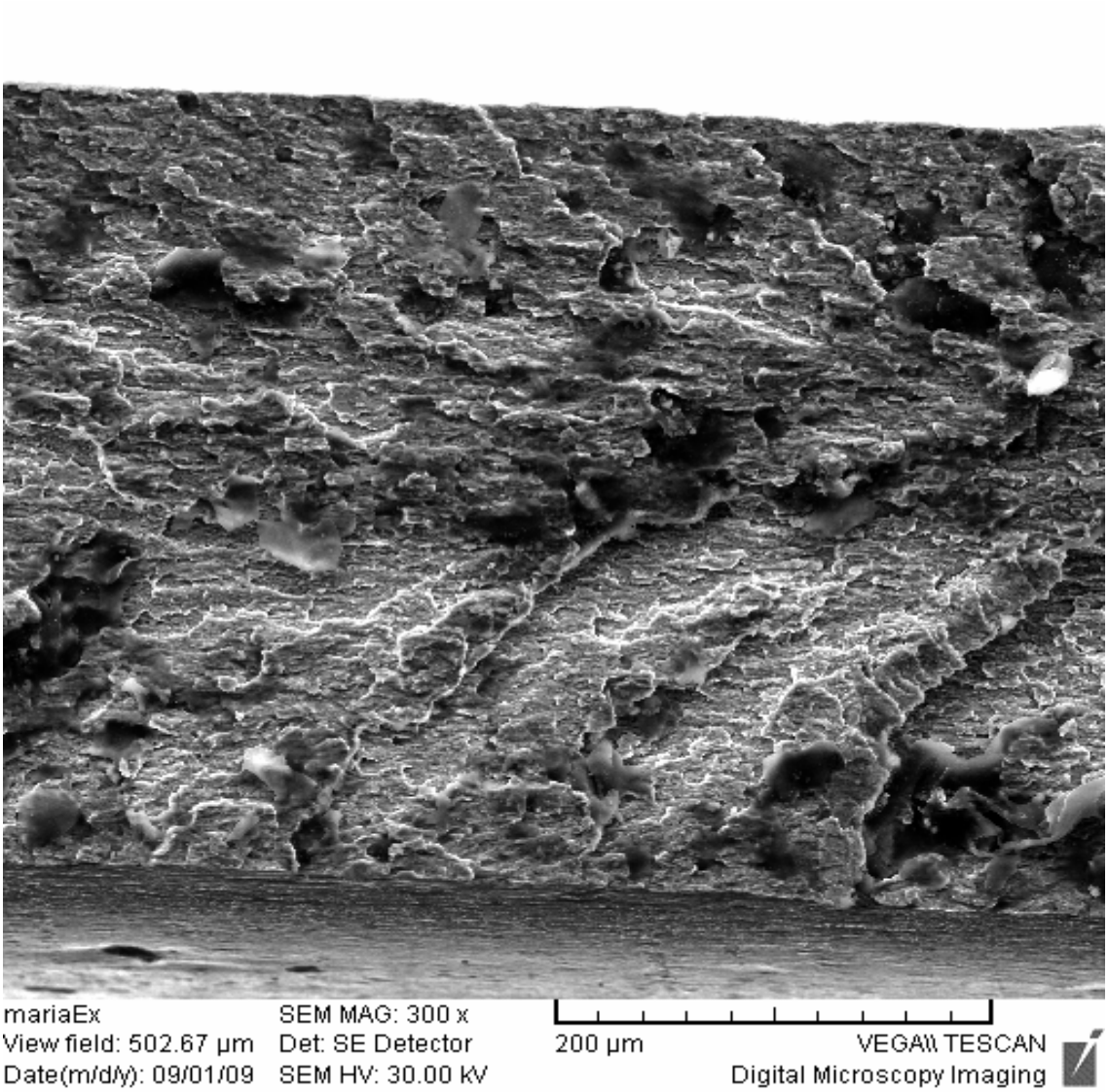

FIG. 3.24. Delayed hydride cracking on specimen A3-5; CANDU Zircaloy tested at 250ºC. Cracking from right to left.

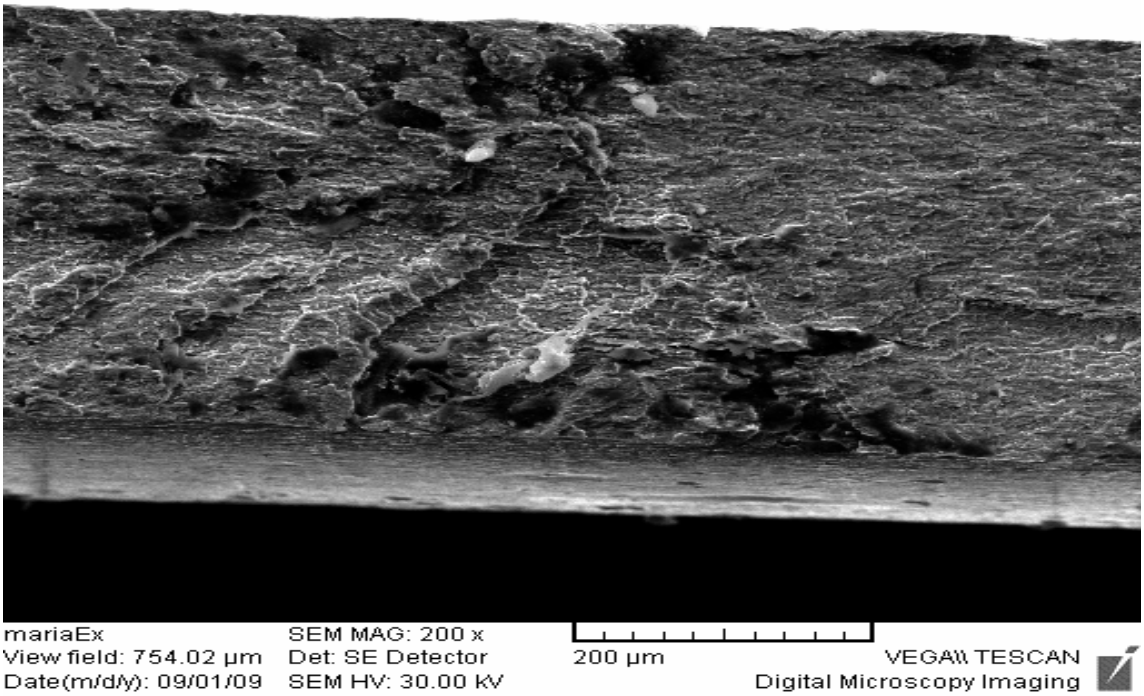

FIG. 3.25. Interface between fatigue pre-crack and DHC on specimen A3-5 CANDU Zircaloy, tested at 250ºC. Cracking from right to left.

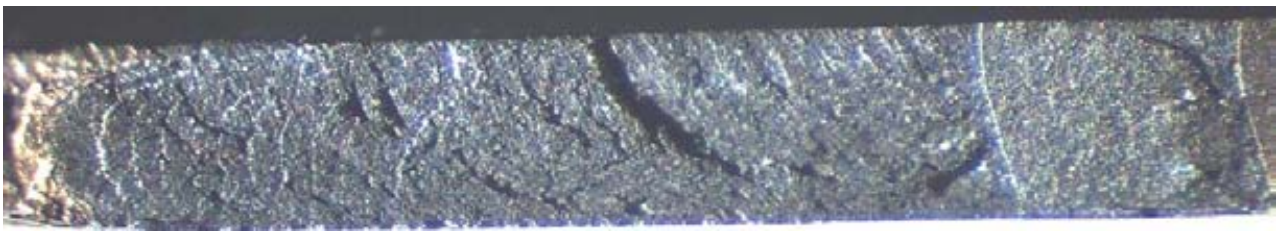

FIG. 3.26. Striations observed on one specimen of CWSR Zircaloy–4 during DHC.

REFERENCE TO CHAPTER 3

[3.1] KEARNS, J.J., Terminal solubility and partitioning of hydrogen in alpha zirconium, Zircaloy-2 and Zircaloy-4, J. Nucl. Mater., **20**, (1967), 292–303.

CHAPTER 4

DISCUSSION

The results presented in Chapter 3 show that this coordinated research programme met its objective. A method of testing fuel cladding for the rate of crack extension, developed in Sweden, has been successfully transferred to several national laboratories. The good agreement on the values between different laboratories on the four main test materials demonstrates the success of this transfer.

The observations from the tests confirmed that Zircaloy–4 fuel cladding could crack by DHC:

— in many tests an incubation time was detected before indications of cracking were observed,
— the crack extended in a stable fashion in the absence of any external chemical assistance, for example, iodine,
— the fracture surface corresponding to DHC was quite distinct from both fatigue and ductile fracture, and was not creep rupture,
— the rates of cracking were in the range expected for DHC,
— the temperature dependence of the crack velocity was also in the range expected, and,
— the crack velocity varied with metallurgical condition.

An expansion of these points follows.

Two batches of cladding were heat-treated to represent PWR cladding. The values of crack velocity, its temperature dependence and the high temperature at which the velocity declined rapidly were all in very good agreement showing that the testing technique is reproducible in the various national laboratories and the materials have similar properties, Fig. 4.1. Specimens from Batch 83786 were tested in three metallurgical conditions: CW, CWSR and RXA. Compared with CWSR material the CW material had similar temperature dependence, but higher values of crack velocity (below 275ºC the average value was about a factor of 1.5 higher) and maybe a slightly higher temperature of decline, 285ºC vs. 275ºC, Fig. 4.2. The behaviour of the RXA material was quite different with a huge scatter providing little chance of discerning any temperature dependence. The values of crack velocity that could be measured were usually much lower than with the CW and CWSR treatments, Fig. 4.3.

The Atucha and CANDU claddings provided similar results, Fig. 4.4, with values much lower than for CWSR material, Fig.4.5.

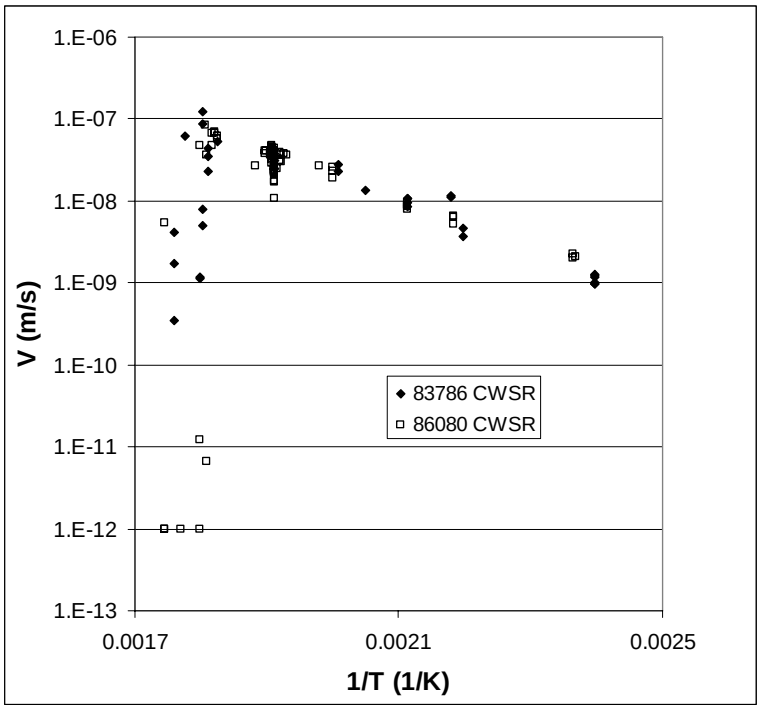

FIG. 4.1. Comparison of DHC behaviour of Zircaloy–4 fuel cladding from Batches 86080 and 83786 in the CWSR condition.

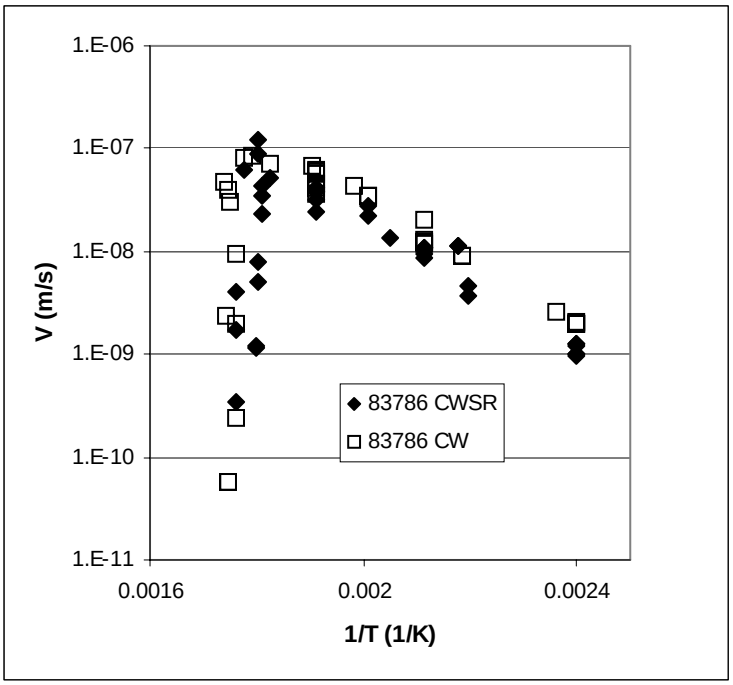

FIG. 4.2. Comparison of DHC behaviour of Zircaloy–4 fuel cladding from Batch 83786 in the CW and CWSR conditions.

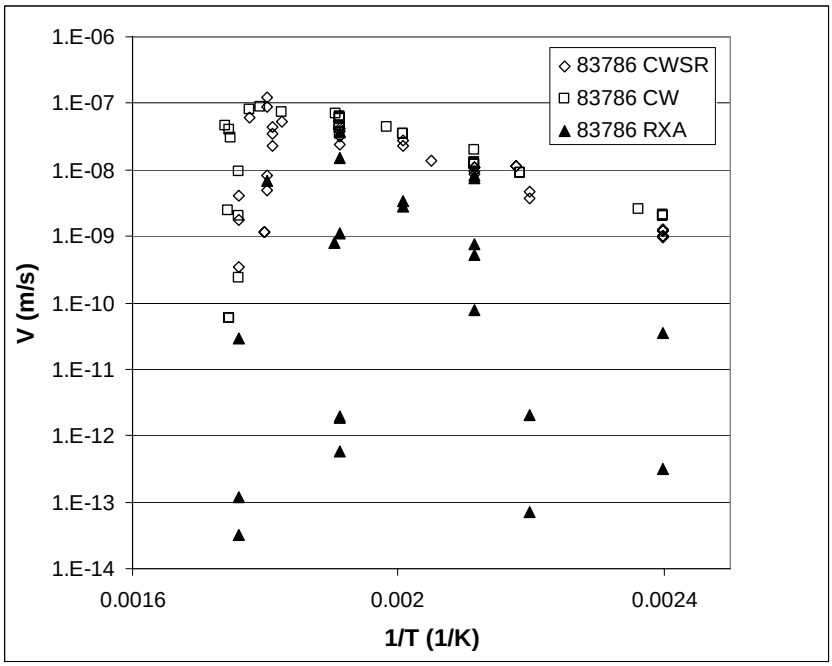

FIG. 4.3. Comparison of DHC behaviour of Zircaloy–4 fuel cladding from Batch 83786 in the CW, CWSR and RXA conditions.

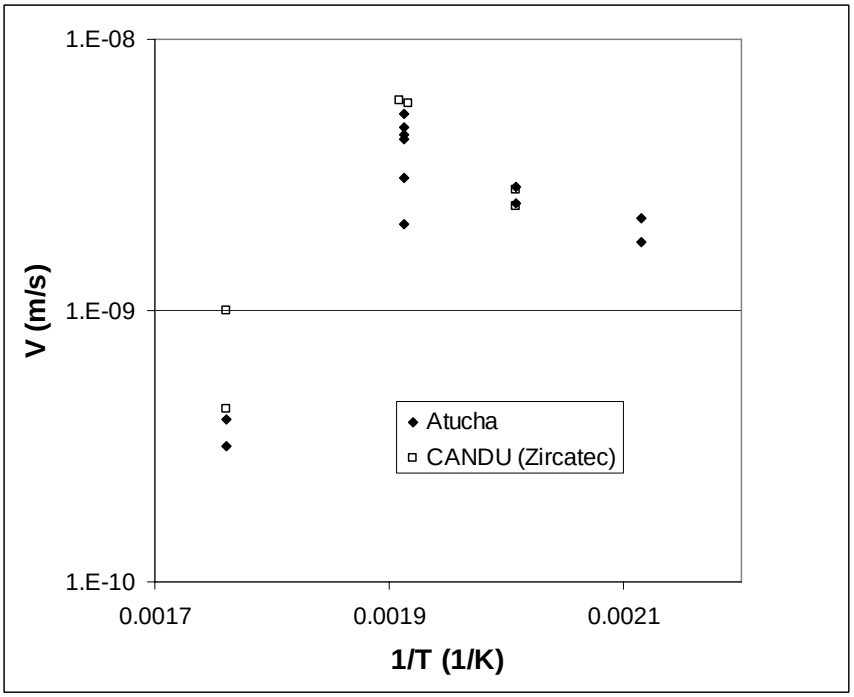

FIG. 4.4. Comparison of DHC behaviour of Zircaloy–4 fuel cladding from Atucha and CANDU (Zircatec).

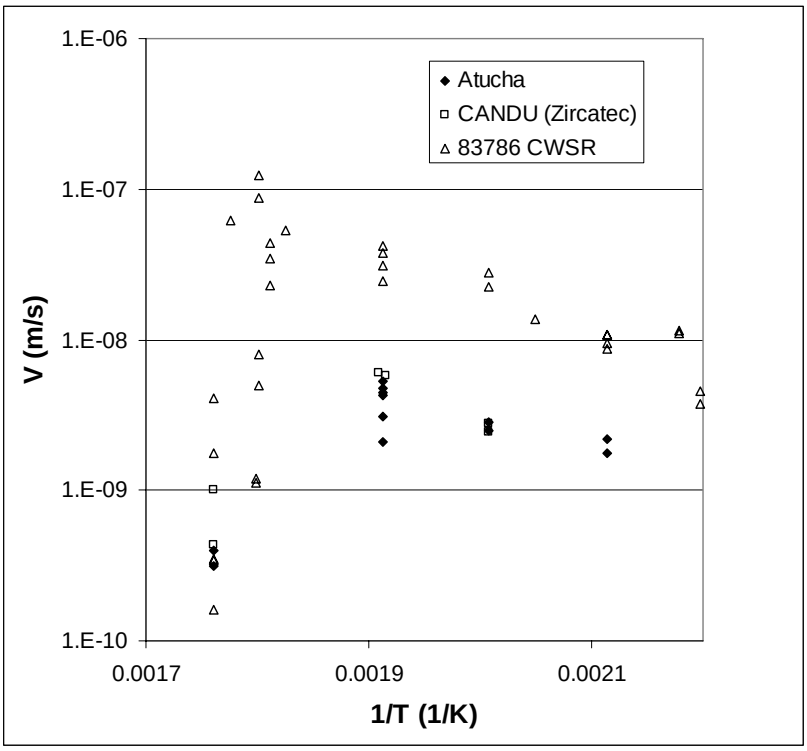

FIG. 4.5. Comparison of DHC behaviour of Zircaloy–4 fuel cladding from Batch 83786 (CWSR), Atucha and CANDU (Zircatec).

The values of V from this study are in agreement with those from measurements on pressure tubes [4.1, 4.2] and on fuel cladding [4.3, 4.4], Fig. 4.6, suggesting similar temperature dependence. The deviations in values can be attributed to:

— differences in the histories of temperature and loading, which can contribute large variations in crack velocity,
— the small number of samples tested; the process of DHC is highly variable and even in well-controlled testing the crack velocity can vary by a factor of three, see Fig. 3.2. Small numbers of specimens may lead to large variations in apparent temperature dependence; for example, the values of Q for the Atucha (Section 3.5.1) and CANDU (Section 3.5.2) materials differ by over a factor of two based on very few points and a narrow temperature range.
— differences in microstructure, including texture, and strength.

A modest correlation is found between UTS and the mean value of V at 250ºC for the current batches of fuel cladding, Fig. 4.7. The temperature dependence of DHC is dominated by the diffusivity, D, and the solubility limit, C, of hydrogen in the zirconium alloy, and to a lesser extent by the strength. Zircaloy–4 is essentially a single-phase alloy, with a distribution of intermetallic particles, and the same values of D and C can be used for all the materials with little error. Comparison with two-phase alloys, like Zr-2.5Nb, has to take into account the distribution of the second phase. Different materials may be compared using the correlation with strength of Oh et al. [4.5] in which V is normalised by the appropriate values of D and C. Fig. 4.8 illustrates the correlation for Batch 86080 with several examples of Zircaloy, both irradiated [4.1, 4.6] and unirradiated, and the samples of Zr-2.5Nb used in the previous IAEA CRP on pressure tube materials [4.7]. UTS was used to characterise strength because that is

the only strength quantity measured in this study. The values of D used for Fig. 4.8 were derived from Sawatzky [4.8] for Zircaloy and [4.9] for Zr-2.5Nb and for C were from Kearns [4.10]. The results for CWSR fuel cladding fit into the broad band of data indicating that the behaviour of fuel cladding is in accord with data from other materials and confirms that material strength contributes to the crack velocity.

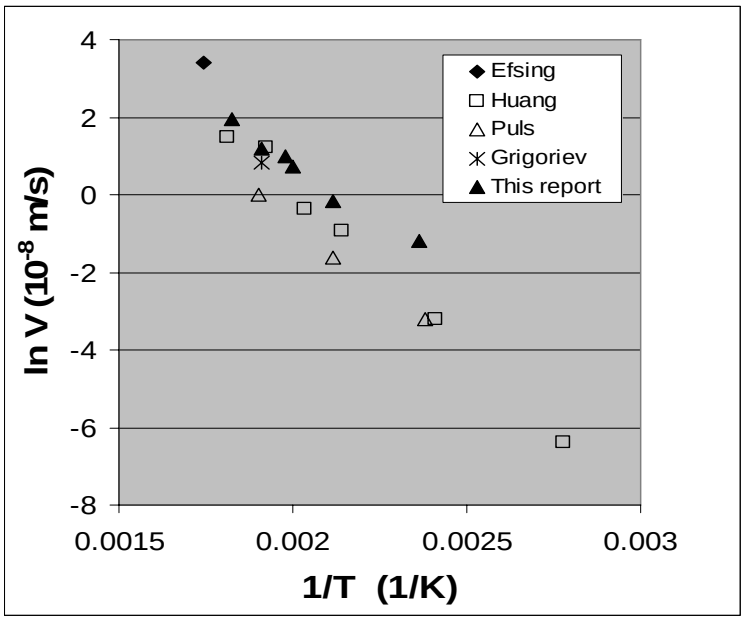

FIG. 4.6. Comparison of temperature dependence the mean values of DHC rate of Batch 86080 Zircaloy–4 cladding with other values on Zircaloy.

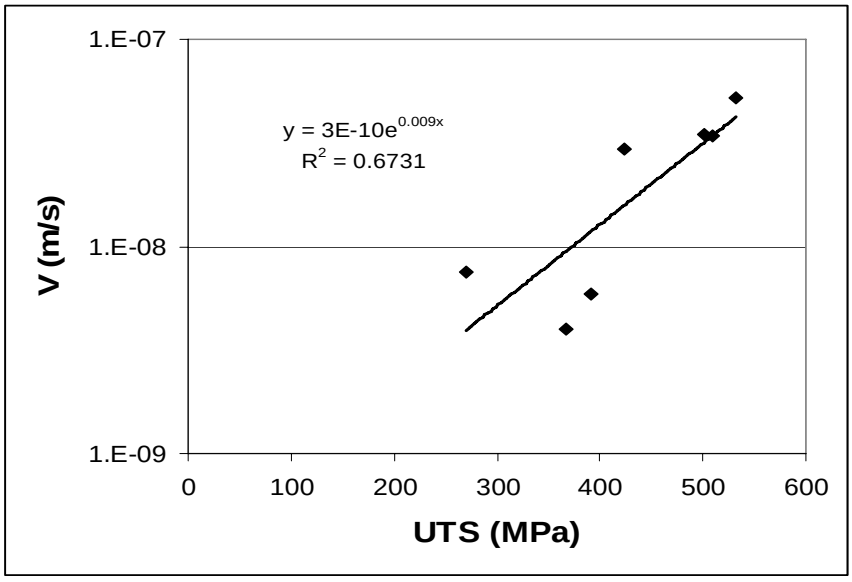

FIG. 4.7. Dependence of V on strength of fuel cladding at 250ºC.

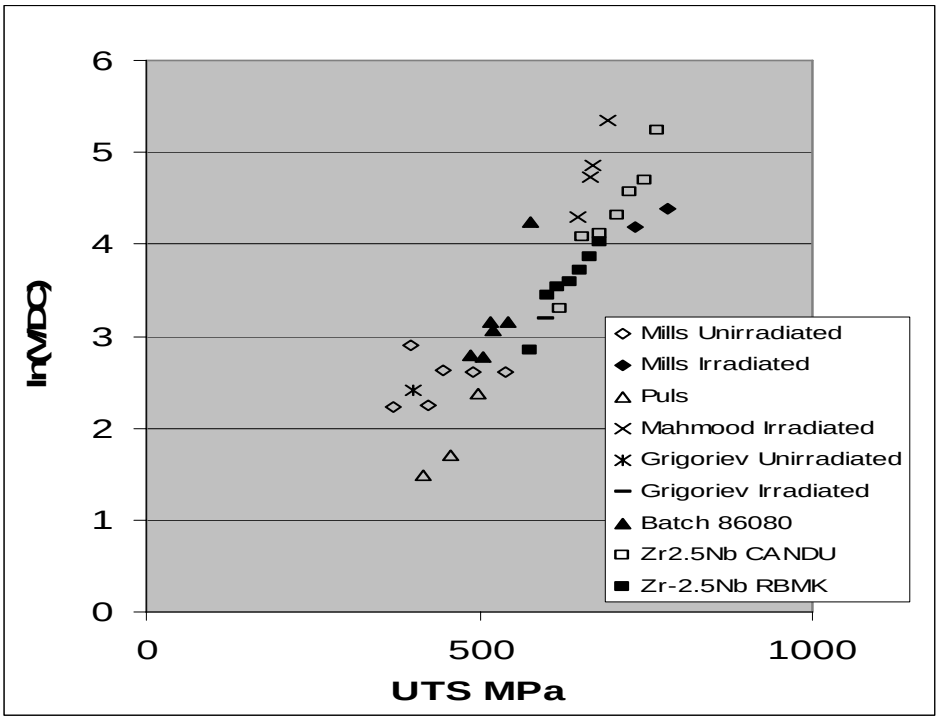

FIG. 4.8. Normalization of DHC velocity, V, with diffusivity, D, and solubility limit for dissolution, C, for zirconium alloys in several conditions.

In Zr-2.5Nb the crack velocity and K_{IH} are very sensitive to crystallographic texture [4.11]. In pressure tubes in the cold worked condition the basal plane normals are strongly oriented in the transverse direction. Cracking in the axial direction driven by a hoop stress is much faster and requires a much lower K_{IH} than cracking in the circumferential direction driven by an axial stress. The explanation is that hydrides reorient readily from the circumferential orientation to the radial direction with a hoop stress but not with an axial stress because the normal to the basal planes of the zirconium crystals, which are close to the habit planes of hydride, are parallel with the hoop direction and not the axial direction. A radial texture has been proposed to protect Zr-2.5Nb from DHC [4.12–4.14]. In all the fuel cladding tested in this study the texture was highly radial (Section 2.2) yet DHC was observed at velocities in line with materials with transverse textures. The α-grains in Zr-2.5Nb are often surrounded by a semi-continuous β-phase and the α-grains tend to be much smaller than those of Zircaloy — 0.2 to 0.5 μm vs. 2 to 3 μm. One possible explanation for the difference in behaviour between the two materials is that the hydrides precipitate in the grain boundaries of Zircaloy and therefore are not affected by the orientation of the α-grains. Metallographic examination of hydrides at the tips of active cracks is required to examine this explanation.

In the usual picture of DHC, after K_{IH} is exceeded, the crack velocity is almost independent of K_I. This conclusion was confirmed for CWSR material — see Figs. 3.5 and 3.6 — the crack velocity of CWSR material was insensitive to K_I and crack length over a wide range of values and indicates that K_{IH} for this material was lower than about 10 MPa√m. The results on RXA material at 250ºC (see the Appendix) indicate that the crack velocity may be highly K_I-dependent, Fig. 4.9, suggesting that K_{IH} is large for this material, perhaps as high as 25 MPa√m. This high sensitivity to K_I may also explain the large variation in values of V obtained in this material and frequent difficulty with initiating cracking.

In this study, the fracture surfaces attributed to DHC were clearly distinct from those made by fatigue or ductile rupture. As previously observed with Zircaloy [4.1, 4.3, 4.4], the fractographic features called striations were absent, except for one observation. These observations are in marked contrast to the fractography of Zr-2.5Nb where striations are easily and often observed. Striations are bands across most of the width of a specimen, perpendicular to the crack growth direction, consisting of regions of ductile fracture bounding cleavage of hydride. They tend to remain a constant width and coplanar as the crack extends. In Zircaloy, the hydrides fracture on different planes along the crack front with ductile fracture between the brittle plates. The size of the brittle areas is variable so bands of consistent width are not formed. This observation supports the idea that the microstructural features contributing to the difference in behaviour of the two materials are probably the finer scale of the grains and the presence of a β-phase in Zr-2.5Nb and the large difference in crystallographic texture — large F_T in pressure tubes and large F_R in fuel cladding. The general lack of striations with DHC in Zircaloy suggests that they are not a fundamental characteristic of DHC.

The decline of DHC at high temperatures has been observed in both Zr-2.5Nb [4.15–4.17] and Zircaloy [4.6]. This feature is apparent in each of the materials tested, except for the RXA material where the scatter obscures any temperature dependence. As an example, Fig. 4.10 is a direct comparison of the behaviour of cold worked Zr-2.5Nb pressure tube material [4.16] and Zircaloy–4 fuel cladding, Batch 83786 in the CW and CWSR conditions. In Zr-2.5Nb the crack velocity starts to deviate from the Arrhenius correlation at about 310°C with no cracking detected at 350°C while in the current Zircaloy–4 the initial deviation is at about 275°C with little or no cracking at 300°C.

The rate of DHC can be suppressed when:

— the hydrogen concentration is insufficient for hydrides to form at the crack tip. The current specimens contained 200 ppm hydrogen, which is sufficient for hydrides to be present at temperatures up to 360 °C, even on cooling to the test temperature. Thus the observed reduced rate of cracking is not caused by lack of hydride.
— the temperature history prevents hydrides from forming at the crack tip. Heating to the test temperatures may cause this situation, even if hydrides are present in the metal matrix [4.18]. In the current tests the test temperature was always attained by cooling from at least 50°C above the test temperature, with no undercooling, so this effect is not the cause of the reduced velocity.
— K_{IH} is greater than the applied K_I.

In Zr-2.5Nb, K_{IH} has little temperature dependence at temperatures below 300°C but at higher temperatures it increases rapidly [4.17]. Zircaloy–4 likely behaves in a similar manner implying that K_{IH} increases to values greater than about 15 MPa$\sqrt{m}$ above 280°C. A corollary to this behaviour is that V and the crack suppression temperature will appear to depend on K_I. Close to the critical temperature, a small amount of evidence supports this conclusion. In Zr-2.5Nb the range of the suppression temperature increased from 280–313°C to 328–359°C when K_I was increase from 13 MPa$\sqrt{m}$ to 17 MPa$\sqrt{m}$ [4.15]. In the current study at 283°C in one specimen no cracking was detected after 9000s at a K_I of 15 MPa$\sqrt{m}$ but once K_I was increased by about 7% the crack progressed, but at a much reduced rate based on expectations from an extrapolation of Equation (1.1).

The maximum value of V in this study was 8.7×10^{-8} m/s at 285°C for CW material, which is four to ten times lower than the rates estimated from splits in LWR cladding [4.19]. The current results are not suitable for direct application to the behaviour of fuel cladding because

the material is unirradiated. The added strength generated by irradiation has two consequences: the crack velocity is increased by a factor between ten to fifty [4.1, 4.4, 4.20] easily agreeing with the rates observed in-reactor, and the high temperature decline in velocity is postponed to higher temperatures [4.17]. Other differences between cladding on an operating fuel element and these laboratory experiments include temperature gradients, which can affect crack velocity and response to temperature history [4.21]. During dry storage of spent fuel, the cladding may reach temperatures of around 400ºC. The high temperature limit suggests that failure by DHC should not be possible for several years as the fuel cools towards the temperatures at which cracking is observed.

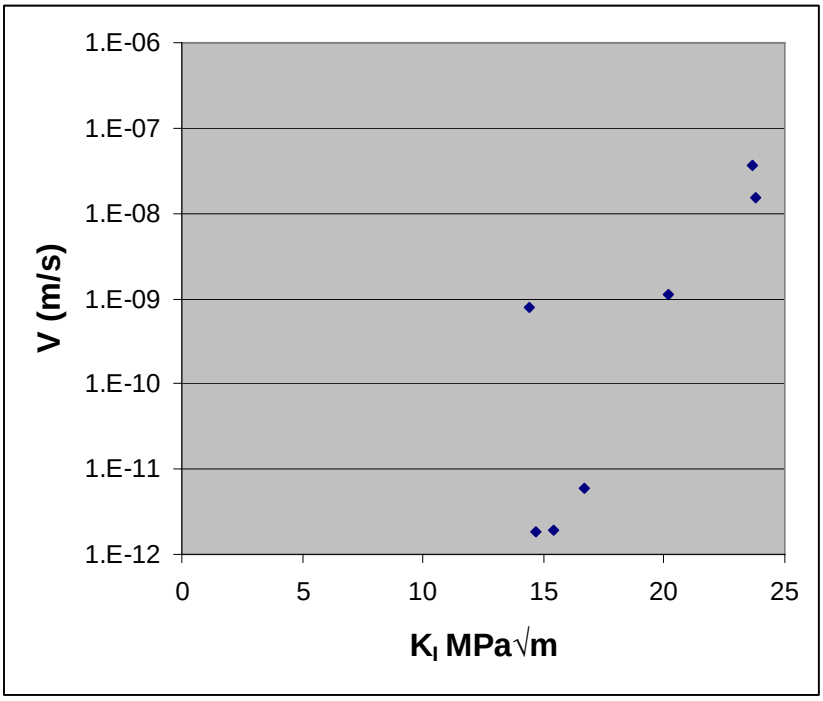

FIG. 4.9. K_I dependence of crack velocity of RXA material at 250ºC.

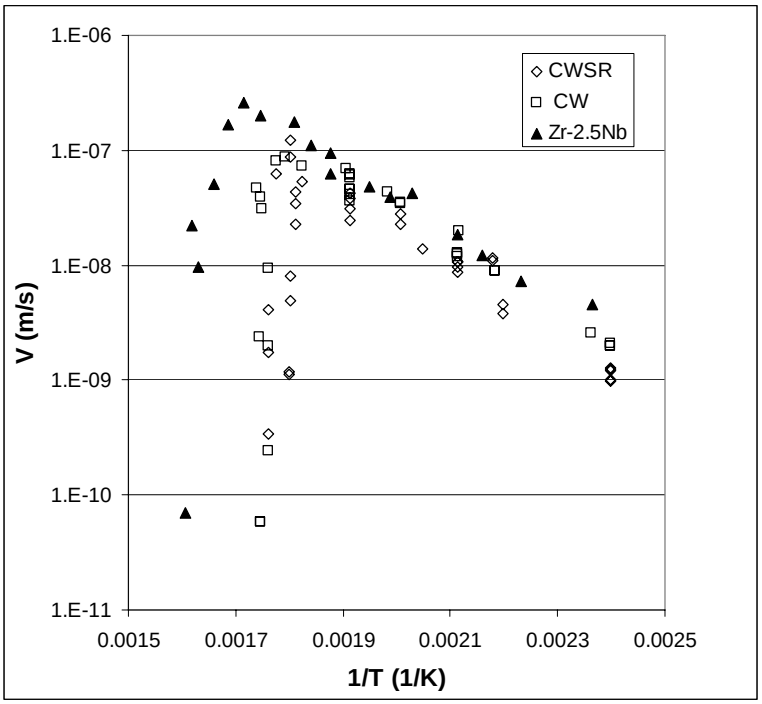

FIG. 4.10. The suppression of DHC in Zr-2.5Nb pressure tube material and Zircaloy–4 fuel cladding (Batch 83786) in the CW and CWSR conditions.

REFERENCES TO CHAPTER 4

[4.1] HUANG, F.H., MILLS, W.J., Delayed hydride cracking behaviour for Zircaloy-2 tubing, Metallurgical Transactions, **22A**, (1991), 2049-2060.

[4.2] PULS, M.P., SIMPSON, L.A., DUTTON, R., Hydride-induced crack growth in Zirconium alloys, AECL Report, AECL-7392, (1982).

[4.3] EFSING, P., PETTERSSON, K., The influence of temperature and yield strength on delayed hydride cracking in hydrided Zircaloy-2, Zirconium in the Nuclear Industry: Eleventh International Symposium, ASTM STP 1295, (1996), 394-404.

[4.4] GRIGORIEV, V., JAKOBSSON, R., Delayed hydrogen cracking velocity and J-Integral measurements on irradiated BWR cladding, Zirconium in the Nuclear Industry: Fourteenth International Symposium, ASTM STP 1467, (2006), 711-728.

[4.5] OH, J.Y., KIM, I.S., KIM, Y.S., A normalization method for relationship between yield stress and delayed hydride cracking velocity in Zr-2.5Nb alloy, J. Nuclear Science and Technology, **37**, (2000), 595-600.

[4.6] MAHMOOD, S.T., FARKAS, D.M., ADAMSON, R.B., ETOH, Y., Post-irradiation characterization of ultra-high-fluence Zircaloy–2 plate, Zirconium in the Nuclear Industry: Twelfth International Symposium, ASTM STP 1354, (2000), 139-169.

[4.7] COLEMAN, C.E., INOZEMSTEV, V.V., Measurement of rates of delayed hydride cracking (DHC) in Zr-2.5Nb – An IAEA Coordinated Research Project, J. ASTM International, 5, Paper ID: 101091, (2008).

[4.8] SAWATZKY, A., The diffusivity and solubility of hydrogen in the alpha-phase of Zircaloy, J. Nuclear Materials, **2**, (1960), 62-68.

[4.9] SAWATZKY, A., LEDOUX, G.A., TOUGH, R.L., CANN, C.D., Hydrogen diffusion in Zirconium-Niobium alloys, Proc. International Symposium on Metal-Hydrogen Systems, Pergamon Press, 109-120, (1981).

[4.10] KEARNS, J.J., Terminal solubility and partitioning of hydrogen in alpha zirconium, Zircaloy-2 and Zircaloy–4, J. Nuclear Materials, **20**, (1967), 292-303.
[4.11] COLEMAN, C.E., Effect of texture on hydride reorientation and delayed hydrogen cracking in cold worked Zr-2.5 Nb, Zirconium in the Nuclear Industry – Fifth International Symposium, ASTM STP 754, (1982), 393-411.
[4.12] COLEMAN, C.E., CHEADLE, B.A., CANN, C.D., THEAKER, J.R., Development of pressure tubes with service life greater than 30 years, Zirconium in the Nuclear Industry – Eleventh International Symposium, ASTM STP 1295, (1996), 884-898.
[4.13] KIM, S.S., KIM, Y.S., K_{IH} in radial textured Zr-2.5%Nb pressure tube, J. Nuclear Materials, **279**, (2000), 286-292.
[4.14] KIM, Y.S., ET AL., Anisotropic threshold stress intensity factor, K_{IH}, and crack growth rate in delayed hydride cracking of Zr-2.5Nb pressure tubes, Met. Mater. Trans., **33**, (2002), 919-925.
[4.15] SMITH, R.R., EADIE, R.L., High temperature limit for delayed hydride cracking, Scripta Metallurgica, **22**, (1988), 833-836.
[4.16] SAGAT, S., PULS, M.P., Temperature limit for delayed hydride cracking in Zr-2.Nb alloys, 17th Inter. Conf. Structural Mechanics in Reactor Technology, Paper G06-4, (2003).
[4.17] RESTA LEVI, M., PULS, M.P., DHC behaviour of irradiated Zr-2.5Nb pressure tubes up to 365 °C, 18th Inter. Conf. Structural Mechanics in Reactor Technology, Paper G10-3, (2005).
[4.18] AMBLER, J.F.R., Effect of direction of approach to temperature on the delayed hydride cracking behaviour of cold worked Zr-2.5Nb, Zirconium in the Nuclear Industry: Sixth International Symposium, ASTM STP 824, (1984), 653-674.
[4.19] EDSINGER, K., A review of fuel degradation in BWRs, Proc. International Topical Meeting on Light Water Reactor Fuel Performance, ANS, Park City, USA, (2000), 162-179.
[4.20] SAGAT, S., COLEMAN, C.E., GRIFFITHS, M., WILKINS, B.J.S., Effect of fluence and irradiation temperature on delayed hydride cracking in Zr-2.5Nb, Zirconium in the Nuclear Industry: Tenth International Symposium, ASTM STP 1245, (1994), 35-61.
[4.21] SAGAT, S., CHOW, C.K., M. P. PULS, M.P., COLEMAN, C.E., Delayed hydride cracking in a temperature gradient, J. Nuclear Materials, **279**, (2000), 107-117.

CHAPTER 5

CONCLUSIONS AND RECOMMENDATIONS

5.1. CONCLUSIONS

(1) The techniques for performing the pin loading tension test for delayed hydride cracking of Zirconium alloy fuel cladding has been transferred from the host laboratory to other countries.
(2) A consistent set of values of crack velocity was obtained by both individual laboratories and between the different laboratories by following a strict testing procedure and paying special attention to test temperatures.
(3) The results fitted into the expected experimental and theoretical framework for delayed hydride cracking of Zircaloy fuel cladding, including the dependence on temperature and strength.
(4) The success of the two CRPs on delayed hydride cracking has stimulated some national programmes.

5.2. RECOMMENDATION

(1) Having established good practice for measuring rates of delayed hydride cracking, the other major parameter for this kind of cracking, the threshold stress intensity factor, K_{IH}, should be evaluated. Both physical importance and experimental complexity of such evaluation are comparable with the work presented above. So the K_{IH} issue might be similarly tackled by a coordinated team of interested labs.

APPENDIX
CRP-II CRACK TESTING DATA

LOT 86080

Lot 86080 **CWSR**	Specimen ID	Hydrogen concentration ppm	Peak temperature °C	Test temperature °C	Initiation time s	Crack length mm	Cracking time s	Crack velocity m/s	Initial K_I MPa√m	Final K_I MPa√m
Romania	S2-2	200	321	251	0	1.717	40969	4.19E-08	14.01	22.21
	S2-3	200	322	251	0	1.952	54244	3.60E-08	15.10	24.87
	S2-5	200	323	251	0	1.589	41248	3.85E-08	16.67	24.80
	S2-6	200	323	251	0	1.386	35615	3.89E-08	15.65	22.49
	S2-7	200	322	251	0	1.767	43728	4.04E-08	17.11	26.30
	S2-8	200	324	251	1800	1.73	39674	4.36E-08	17.20	26.20
	S2-9	200	322	251	0	1.86	43155	4.31E-08	14.75	23.93
	S2-10	200	324	251	3420	1.631	36224	4.50E-08	16.03	24.27
	S2-11	200	323	251	2280	1.527	46434	3.29E-08	16.57	24.35
	S2-12	200	322	251	372	1.75	42147	4.15E-08	15.66	24.46
	S2-13	200	323	251	30	1.693	45713	3.70E-08	17.23	26.03
	S2-14	200	320	251	1200	1.957	51382	3.81E-08	16.81	26.99
	S2-15	200	322	251	4440	1.706	43374	3.93E-08	16.38	25.09
Lithuania	LT_S7-1	200	315	250	5340	2.83	79380	3.57E-08	14.69	28.54
	LT_S7-2	200	315	250	10200	1.71	52080	3.28E-08	13.91	21.82
	LT_S7-3	200	315	250	4200	3.29	79320	4.15E-08	14.04	30.05
	LT_S7-4	200	315	250	8100	2.09	63180	3.31E-08	14.57	24.52
	LT_S7-5	200	315	250	2520	2.47	69480	3.55E-08	15.28	27.39
	LT_S7-6	200	315	250	4500	2.57	67980	3.78E-08	14.52	26.97
	LT_S7-7	200	315	250	2940	2.52	61920	4.07E-08	15.28	27.65
	LT_S7-8	200	315	250	7320	2.41	66000	3.65E-08	14.82	26.55
	LT_S7-9	200	285	200	20820	2.12	249120	8.51E-09	14.32	24.37
	PLT_S7-3	200	285	200	0	1.84	234540	7.85E-09	14.16	22.73
	LT_S7-10	200	333	275	61680	1.59	26040	6.11E-08	15.6	23.5
	LT_S7-11	200	333	283	95100	0.001	95100	no cracking	17.7	-

	LT_S7-12	200	333	283	8700	1.67	35820	4.66E-08	15.78	24.09
Sweden	S1-1	200	315	246.2	3720	2.76	73530	3.75E-08	14.5	27.9
	S1-2	200	315	247.9	2580	2.89	74340	3.9E-08	13.4	27.1
	S1-4a	200	315	253.9	0	2.78	68460	4.1E-08	15.2	28.8
	S1-5	200	315	244.8	2760	2.81	76470	3.7E-08	16.0	30.0
	S1-7	200	315	253.6	720	2.80	69870	4.0E-08	13.9	27.3
	S1-8	200	315	251.7	1800	2.80	68910	4.1E-08	14.7	28.3
	S12-5	200	400	232	0	1.93	72540	2.7E-08	11.9	20.2
	S12-6_2	200	400	300.1	0	0.59	107160	5.5E-09	15.5	18.0
	S12-8_1	200	400	280.6	0	2.42	28680	8.4E-08	11.9	22.6
	S12-8_2	200	400	149.4	0	0.92	440820	2.1E-09	19.6	23.7
Brazil	A1	200	320	250	16200	2.252	87420	2.58E-08	15.7	26.2
	S4-B	200	320	250	14400	1.704	79200	2.15E-08	16.9	25.2
	S4-C	200	320	250	18000	2.054	78360	2.62E-08	14.8	24.5
	S4-3	200	320	250	10800	2.38	108000	2.20E-08	17.5	29.3
Russian	925	200	315	250	8100	2.425	140700	1.72E-08	19.9	36.7
Federation	927	200	315	250	1800	2.096	82200	2.55E-08	18.5	31.6
	930	200	315	250	300	1.844	81000	2.28E-08	19.2	30.7
	914	200	315	247	4350	2.317	76590	3.03E-08	22.8	38.9
	922	200	315	248	210	2.571	82620	3.11E-08	19.1	28.3
	915	200	315	185	15360	1.188	224820	5.28E-09	21.5	29.8
	919	200	315	185	96960	2.53	400800	6.31E-09	22.5	38.3
	920	200	315	185	153180	1.354	210330	6.44E-09	18.5	26.7
	916	200	350	275	6300	3.365	58500	5.75E-08	19.7	42.7
	917	200	350	277	15300	3.178	66000	4.82E-08	19.9	41.2
	924	200	350	277	19800	3.078	46800	6.58E-08	17.2	35.6
	918	200	350	280	11400	2.681	73500	3.65E-08	19.6	37.6
	923	200	350	280	152220	0.001	152220	6.57E-12	19.0	-
	928	200	351	283	82200	0.001	82200	1.22E-11	18.0	-
	921	200	350	292	1019220	0.001	1019220	9.81E-13	18.0	-
Korea,	I-3C	200	317	258	17880	3.29	124800	2.64E-08	13	30.5
Rep. of	I-3a	200	317	254	3780	2.21	57480	3.84E-08	13.7	24.2
	S3-2	200	311	247	4260	1.69	46800	3.61E-08	13.9	21.8
	I-3f	200	315	252	960	2.13	58560	3.64E-08	13.7	23.8
	S3-3	200	318	251	2700	2.49	63600	3.92E-08	13.4	25.3
	I-2a	200	323	251	6120	1.74	59460	2.93E-08	12.4	21.1

	I-2b	200	311	251	1500	2.25	63160	3.56E-08	14.1	24.9
	S13b	200	365	276	34740	2.94	44280	6.64E-08	13.4	25.4
	S13e	200	365	276	32380	3.57	51840	6.89E-08	13.1	27.8
	S11b	200	315	150	72720	0.55	269100	2.04E-09	14.5	16.6
	S13x	200	325	150	61260	0.6	263520	2.28E-09	12.2	14.2
India	S6-2	200	315	250	600	3.018	84600	3.60E-08	13.42	27.74
	S6-3	200	315	250	2400	4.125	149400	2.76E-08	12.99	32.12
	S6-I3	200	315	250	3600	2.965	86400	3.43E-08	15.59	29.68
	S6-I4	200	315	250	0	2.465	66600	3.70E-08	15.03	26.56
	S6-I6	200	315	250	600	2.725	72000	3.78E-08	14.11	26.73
	S6-I7	200	315	250	0	2.605	66600	3.91E-08	14.62	26.76
	S6-I8	200	315	250	1800	2.59	68400	3.78E-08	13.24	24.96
	S6-I9	200	315	250	1200	2.535	72000	3.52E-08	14.99	26.86
	S6-I10	200	315	200	900	1.95	230400	8.9E-09	15.62	24.71
	S6-I11	200	315	200	1200	1.56	160200	9.69E-09	16.26	23.51
Pakistan	PLT-1	200	315.0	249	303.60	4.169	167113.80	2.495E-08	14.44	34.95
	PLT-2	200	316.5	250	4140.00	3.608	106200.00	3.397E-08	11.58	28.26
	PLT-3	200	316.0	250	3399.00	2.507	60480.00	4.145E-08	11.72	22.79
	PLT-4	200	317.8	251	5022.00	2.646	56100.00	4.717E-08	13.21	25.6
	PLT-5	200	312.7	250	6175.20	2.368	54780.00	4.323E-08	13.77	24.91
	PLT-6	200	319.7	250	2275.80	2.040	61440.00	3.320E-08	15.72	25.64
	PLT-A	200	316.6	250	3780.00	2.189	55612.20	3.936E-08	14.20	24.54
	PLT-B	200	317.9	250	9231.00	2.311	55920.00	4.133E-08	13.21	23.87
150N	PLT-7	200	351.4	300	44940.00	-	-	1.000E-12	21.12	21.12
200N	PLT-7a	200	351.4	300	46500.00					
	PLT-8	200	302.4	227	12312.00	1.582	61776.00	2.561E-08	15.78	23.35
	PLT-9	200	303.0	227	5040.00	1.560	67824.00	2.300E-08	16.53	24.11
	PLT-10	200	300.0	227	17388.00	1.335	69012.00	1.934E-08	15.77	22.09
Argentina	S5-2	200	315	250	0	3.69	155440	2.38E-08	14.1	32.2
	S5-3	200	315	250	6900	2.8	167550	1.67E-08	14.1	27.6
	SA-1	200	315	250	5200	2.08	82330	2.52E-08	14.2	24
	SA-2	200	315	250	4100	2.66	92580	2.87E-08	12.8	25.1
	SA-3	200	315	250	0	3.19	141610	2.25E-08	14.4	30
	SA-4	200	315	250	0	1.47	138190	1.06E-08	13.8	20.4
	SA-5	200	315	250	2900	2.42	113870	2.13E-08	11	21.6
	SA-6	200	315	250	0	3.05	130490	2.34E-08	16.6	33.5

LOT 83786

Lot 83786 Cold worked	Specimen ID	Hydrogen concentration ppm	Peak temperature °C	Test temperature °C	Initiation time s	Crack length mm	Cracking time s	Crack velocity m/s	Initial K_I MPa√m	Final K_I MPa√m
Romania	S71-1	206	334	225	3600	1.2	33900	3.54E-08	14.62	19.69
	S71-2	206	334	225	219000	1.04	30341	3.43E-08	16.86	21.44
	S71-3	206	344	295	10260	0.17	85383	1.99E-09	12.65	13.27
	S71-4	206	344	295	295800	2.03	217096	9.35E-09	13.16	21.71
Lithuania	51_2	200	315	250	0	1.45	23160	6.26E-08	13.95	20.32
	51_3	200	315	250	0	1.5	24720	6.07E-08	13.76	20.37
	51_4	200	315	250	0	1.69	29520	5.72E-08	14.28	22.12
Sweden	CW2	200	400	251.8	0	4.13	59640	6.9E-08	17.1	36.6
	CW3	200	400	231.1	0	2.28	53100	4.3E-08	13.8	24.1
	CW4	200	400	300.7	0	0.6	254520	2.4E-09	12.4	14.7
	CW4a (1)	200	400	199.8	0	1.5	76680	2.0E-08	15.7	21.9
	CW4a (2)	200	400	150.4	0	0.63	239760	2.6E-09	21.9	24.6
Russian	814	200	315	250	300	2.474	60300	4.10E-08	22.6	36.7
Federation	8110	200	315	250	6900	2.552	55500	4.60E-08	16.4	30.9
	816	200	315	185	27900	1.443	161400	8.94E-09	16.4	23.6
	817	200	315	185	1200	1.696	190800	8.89E-09	17.6	27.1
	812	200	350	275	2100	2.656	36900	7.20E-08	16.5	31.1
	819	200	350	285	300	1.686	19500	8.65E-08	18.5	27.6
	811	200	350	290	300	1.619	19800	8.18E-08	16.5	25.4
	8112	200	350	295	414720	0.1	414720	2.41E-10	18.0	…
Korea,	#41-1	200	377	302	24420	2.12	45180	4.69E-08	13.2	21.6
Rep. of	#41-2	200	365	300	23760	2.26	35820	3.96E-08	14.2	23.4
	#41-3	200	362	299	22560	1.76	165240	3.08E-08	14.7	26.2
	#41-4	200	365	300	172800	0.01	172800	5.79E-11	14.7	…
	#41-5	200	400	300	172800	0.01	172800	5.79E-11	14.7	…
India	31A2	190	315	250	4200	2.161	60480	3.60E-08	14.88	25.68
	31B2	240	315	144	8100	0.868	424800	2.00E-09	18.91	22.76

	31B4	240	315	200	4200	2.046	165600	1.24E-08	21.83	33
	31B5	240	315	200	3300	2.184	169200	1.29E-08	21.39	33.31
	31C1	188	315	250	1620	4.023	87300	4.60E-08	15.59	36.75
	31C2	188	315	200	3780	1.684	140400	1.20E-08	20.3	29.39
	31C3	188	315	144	8400	1.225	604800	2.00E-09	20.15	20.88
	31C4	188	315	144	7200	0.725	345600	2.1E-09	18	19.94

Lot 83786 CWSR	Specimen ID	Hydrogen concentration ppm	Peak temperature ^{o}C	Test temperature ^{o}C	Initiation time s	Crack length mm	Cracking time s	Crack velocity m/s	Initial K_I MPa$\sqrt{m}$	Final K_I MPa$\sqrt{m}$
Romania	S72-1	219	334	225	0	1.3	57314	2.27E-08	14.11	19.55
	S72-2	219	335	225	0	1.36	48731	2.79E-08	13.65	19.29
	S72-3	219	336	295	0	0.34	82673	4.11E-09	13.20	14.50
	S72-4	219	336	295	0	0.16	91779	1.74E-09	12.47	13.05
Lithuania	52_1	200	285	200	5880	1.58	165240	9.56E-09	13.52	20.47
	52_2	200	285	200	900	1.67	156480	1.07E-08	13.76	21.19
	52_3	200	333	283	11760	0.42	371280	1.13E-09	14.44	16.3
	52_4	200	333	275	0	1.6	30120	5.31E-08	13.29	20.23
	52_5	200	333	279	0	1.34	58440	2.29E-08	13.72	19.56
	52_6	200	333	279	0	1.56	45240	3.45E-08	13.8	20.71
	52_7	200	333	279	900	1.67	38400	4.35E-08	14.43	22.02
	52_8	200	285	200	0	1.6	183900	8.70E-09	13.72	20.8
	52_9	200	275	144	10440	1.52	1268040	1.20E-09	13.41	20.04
	52_10	200	275	144	11400	1.79	1443660	1.24E-09	13.72	21.72
	52_11	200	333	283	0	0.4	338400	1.18E-09	15.37	17.16
India	32A4	245	315	144	7200	0.231	234000	9.87E-10	20.9	22.1
	32B4	209	315	144	7500	0.63	496800	1.27E-09	24.14	27.6
	32B5	209	315	144	7800	0.54	540000	1.00E-09	24.39	27.33
	32C1	212	315	282	16680	0.36	44700	8.05E-09	19.67	21.52
	32C2	212	315	250	2700	2.98	70320	4.24E-08	15.9	31.5
	32C3	212	315	282	7800	0.66	133200	4.95E-09	15.19	18.2
	32C4	212	315	250	2400	2.86	75360	3.80E-08	17.14	32.3
	32C5	212	315	200	2400	1.81	169200	1.07E-08	19.5	29.1

Pakistan										
250N	PWR-1B	215	370.4	295	29040	0.010	-	3.44E-10	22.88	22.88
300N	PWR-1Ba	215	370.4	295	28800			3.47E-10		
350N	PWR-1Bb	215	370.4	295	62100			1.61E-10		
	PWR-2B	220	259.7	186	20376	2.118	190512	1.11E-08	22.40	40.93
	PWR-3B	210	259.0	186	360	2.105	183600	1.15E-08	22.48	40.95
Russian Federation	82-03/SRA	200	350.0	282	300	1.144	9300	1.23E-07	25.00	32
	82-06/SRA	200	315.0	250	7200	1.723	55200	3.12E-08	16.00	25.4
	82-11/SRA	200	315.0	250	4800	4.725	193500	2.44E-08	16.50	44.6
	82-07/SRA	200	315.0	182	48000	1.997	532800	3.75E-09	17.50	29.1
	82-10/SRA	200	315.0	182	132600	1.276	277800	4.59E-09	15.00	22.8
	82-10_2/SRA	200	350.0	282	300	0.605	6900	8.77E-08	24.70	28.5
	82-2/SRA	200	300.0	144	196500	1.310	1337700	9.79E-10	17.90	25.4
	82-2_2/SRA	200	350.0	290	300	1.018	16500	6.17E-08	24.00	30
	82-4/SRA	200	350.0	215	27840	1.929	140400	1.37E-08	17.80	29.1

Lot 83786 RXA	Specimen ID	Hydrogen concentration ppm	Peak temperature °C	Test temperature °C	Initiation time s	Crack length mm	Cracking time s	Crack velocity m/s	Initial K_I MPa√m	Final K_I MPa√m
Romania	S73-1	193	333	225	0	0.66	236342	2.79E-09	14.42	17.12
	S73-2	193	333	225	4173	1.15	341770	3.36E-09	14.03	18.80
Lithuania	53_1	200	315	250	546600	0.001	546600	1.83E-12	14.7	-
	53_2	200	315	250	514260	0.001	514260	1.94E-12	15.4	-
	53_3	200	285	200	0	0.28	3546720	7.89E-11	14.19	21.15
Sweden	53-1s	200	320	252.3	0	0.15	191280	7.84E-10	14.4	15.1
Russian Federation	831	200	315	182	499440	0.001	499440	2.00E-12	16	
	832	200	315	182	1434540	0.0001	1434540	6.97E-14	18	
	8322	200	350	295	858480	0.0001	858480	1.16E-13	18	
	833	200	350	295	300	0.067	2332920	2.87E-11	18.4	
	838	200	350	295	3185700	0.0001	3185700	3.14E-14	14	
India	33A3	206	315	144	324000	0.001	324000	3.09E-13	16.1	

33A4	206	315	250	169200	0.001	169200	5.91E-13	16.7	
33A5	206	315	200	1800	0.075	97740	7.6E-10	16.95	17.3
33B1	280	315	282	6900	0.585	86400	6.8E-09	23.56	26.75
33B2	280	315	200	1980	1.34	187200	7.4E-09	20.2	27.6
33B3	280	315	250	2400	2.314	64800	3.60E-08	23.68	36.33
33B4	280	315	250	3000	1.543	104400	1.50E-08	23.8	32.3
33B5	280	315	200	2400	0.075	144000	5.2E-10	18.15	19.41
33B5r	280	315	200	1800	2.046	252000	8.1E-09	20.12	31.2
33C3	238	315	250	3000	0.143	126000	1.1E-09	20.15	20.88
33C4	238	315	144	1800	0.018	507600	3.5E-11	16.6	19.69

ATUCHA Lot MA-61

ATUCHA Lot MA-61	Specimen ID	Hydrogen concentration ppm	Peak temperature °C	Test temperature °C	Initiation time s	Crack length mm	Cracking time s	Crack velocity m/s	Initial K_I MPa√m	Final K_I MPa√m
Romania	A1-3	212	321	225	7032	0.85	299215	2.84E-09	13.80	17.40
	A1-4	212	318	225	32856	0.94	376500	2.50E-09	13.68	17.68
	A1-1	212	321	250	63802	1.09	228842	4.76E-09	13.45	18.09
	A1-2	212	320	250	8703	1.08	252225	4.28E-09	14.81	19.63
	A2-1	212	352	295	5253	0.1	252267	3.96E-10	15.69	16.12
	A2-2	212	355	295	10776	0.1	318087	3.14E-10	16.60	17.05
India	ArgB1	210	315	250	9780	0.415	78360	5.3E-09	18.3	20.4
	ArgB2	210	315	250	18000	0.583	130800	4.46E-09	15.53	18.23
	ArgC1	258	315	250	9300	0.501	162000	3.1E-09	15.9	18.2
	ArgC2	258	315	200	9960	0.225	126000	1.78E-09	15.54	16.56
	ArgC3	258	315	200	10200	0.44	190800	2.18E-09	15.25	17.24
	ArgC4	258	315	250	7200	0.469	225600	2.08E-09	17.8	20.16

CANDU Lot 226289

CANDU Zircatec Lot 226289	Specimen ID	Hydrogen concentration ppm	Peak temperature °C	Test temperature °C	Initiation time s	Crack length mm	Cracking time s	Crack velocity m/s	Initial K_I MPa√m	Final K_I MPa√m
Romania	C1-3	208	321	225	7742	0.94	339061	2.77E-09	15.84	20.57
	C1-4	208	318	225	23391	0.78	323303	2.41E-09	16.16	20.09
	C1-1	208	320	250	15493	0.69	115463	5.98E-09	15.79	19.19
	C1-2	208	321	250	13581	0.78	133988	5.82E-09	16.92	20.96
	C1-5	208	362	295	51224	0.15	347246	4.32E-10	16.83	17.56
	C1-6	208	361	295	1470	0.32	321453	9.95E-10	16.16	17.71

CANDU Lot 80642

CANDU Sandvik Lot 80642	Specimen ID	Hydrogen concentration ppm	Peak temperature °C	Test temperature °C	Initiation time s	Crack length mm	Cracking time s	Crack velocity m/s	Initial K_I MPa√m	Final K_I MPa√m
Romania	A3-1	202	315	249	0	3.97	162036	2.45E-08	15.44	38.15
	A3-2	202	318	249	0	3.56	133387	2.67E-08	16.63	37.23
	A3-3	202	321	249	0	2.52	77569	3.25E-08	18.36	33.01
	A3-4	202	315	249	66266	2.15	54794	3.92E-08	17.24	29.36
	A3-5	202	318	249	0	2.48	98187	2.53E-08	18.84	33.35

CONTRIBUTORS TO DRAFTING AND REVIEW

Adelfang, P.	International Atomic Energy Agency
Ali, L.	Pakistan Institute of Nuclear Science and Technology, Pakistan
Azhar, T.	Pakistan Institute of Nuclear Science and Technology, Pakistan
Baltusnikas, A.	Lithuanian Energy Institute, Lithuania
Batista de Lima, N.	Instituto de Pesquisas Energéticas e Nucleares, Brazil
Bipeta, C.	Bhabha Atomic Research Centre, India
Buyers, A.	Atomic Energy of Canada Limited, Canada
Chakravartty, J.	Bhabha Atomic Research Centre, India
Cheong, Y.M.	Korea Atomic Energy Research Institute, Republic of Korea
Coleman, C.E.	Atomic Energy of Canada Limited, Canada
Correa, O.	Instituto de Pesquisas Energéticas e Nucleares, Brazil
Dubey, J.	Bhabha Atomic Research Centre, India
Fernàndez, S.	Comisión Nacional de Energía Atómica, Argentina
Grigoriev, V.	Studsvik Nuclear, Sweden
Grybenas, A.	Lithuanian Energy Institute, Lithuania
Haddad, R.	Comisión Nacional de Energía Atómica, Argentina
He, Z.	Atomic Energy of Canada Limited, Canada
Homobono Paes de Andrade, A.	Instituto de Pesquisas Energéticas e Nucleares, Brazil
Kim, K.S.	Korea Atomic Energy Research Institute, Republic of Korea
Inozemtsev, V.	International Atomic Energy Agency
Ionescu, V.	Institute for Nuclear Research, Romania
Jakobsson, R.	Studsvik Nuclear, Sweden
Khan, A.	Pakistan Institute of Nuclear Science and Technology, Pakistan
Kim, Y.S.	Korea Atomic Energy Research Institute, Republic of Korea
Kotov, P.	A.A. Bachavar, All-Russian Scientific Research Institute of Inorganic Materials, Russian Federation
Kriukiene, R.	Lithuanian Energy Institute, Lithuania
Kulavil, M.	Bhabha Atomic Research Centre, India
Lafont, C.	Comisión Nacional de Energía Atómica, Argentina

Lidström, O.	Studsvik Nuclear, Sweden
Lockley, A.	Atomic Energy of Canada Limited, Canada
Makarevicius, V.	Lithuanian Energy Institute, Lithuania
Manzoor, T.	Pakistan Institute of Nuclear Science and Technology, Pakistan
Markelov, V.	A.A. Bachavar, All-Russian Scientific Research Institute of Inorganic Materials, Russian Federation
Mihalache, M.	Institute for Nuclear Research, Romania
Mizrahi, R.	Comisión Nacional de Energía Atómica, Argentina
Pitigoi, V.	Institute for Nuclear Research, Romania
Pizarro, L.M.	Comisión Nacional de Energía Atómica, Argentina
Ramanathan, L.	Instituto de Pesquisas Energéticas e Nucleares, Brazil
Roth, M.	Institute for Nuclear Research, Romania
Tsvelev, V.	A.A. Bachavar, All-Russian Scientific Research Institute of Inorganic Materials, Russian Federation
Zheltkovskaya, T.	A.A. Bachavar, All-Russian Scientific Research Institute of Inorganic Materials, Russian Federation

No. 21, July 2006

IAEA
International Atomic Energy Agency

Where to order IAEA publications

In the following countries IAEA publications may be purchased from the sources listed below, or from major local booksellers. Payment may be made in local currency or with UNESCO coupons.

Australia
DA Information Services, 648 Whitehorse Road, Mitcham Victoria 3132
Telephone: +61 3 9210 7777 • Fax: +61 3 9210 7788
Email: service@dadirect.com.au • Web site: http://www.dadirect.com.au

Belgium
Jean de Lannoy, avenue du Roi 202, B-1190 Brussels
Telephone: +32 2 538 43 08 • Fax: +32 2 538 08 41
Email: jean.de.lannoy@infoboard.be • Web site: http://www.jean-de-lannoy.be

Canada
Bernan Associates, 4611-F Assembly Drive, Lanham, MD 20706-4391, USA
Telephone: 1-800-865-3457 • Fax: 1-800-865-3450
Email: order@bernan.com • Web site: http://www.bernan.com

Renouf Publishing Company Ltd., 1-5369 Canotek Rd., Ottawa, Ontario, K1J 9J3
Telephone: +613 745 2665 • Fax: +613 745 7660
Email: order.dept@renoufbooks.com • Web site: http://www.renoufbooks.com

China
IAEA Publications in Chinese: China Nuclear Energy Industry Corporation, Translation Section, P.O. Box 2103, Beijing

Czech Republic
Suweco CZ, S.R.O. Klecakova 347, 180 21 Praha 9
Telephone: +420 26603 5364 • Fax: +420 28482 1646
Email: nakup@suweco.cz • Web site: http://www.suweco.cz

Finland
Akateeminen Kirjakauppa, PL 128 (Keskuskatu 1), FIN-00101 Helsinki
Telephone: +358 9 121 41 • Fax: +358 9 121 4450
Email: akatilaus@akateeminen.com • Web site: http://www.akateeminen.com

France
Form-Edit, 5, rue Janssen, P.O. Box 25, F-75921 Paris Cedex 19
Telephone: +33 1 42 01 49 49 • Fax: +33 1 42 01 90 90 • Email: formedit@formedit.fr

Lavoisier SAS, 14 rue de Provigny, 94236 Cachan Cedex
Telephone: + 33 1 47 40 67 00 • Fax +33 1 47 40 67 02
Email: livres@lavoisier.fr • Web site: http://www.lavoisier.fr

Germany
UNO-Verlag, Vertriebs- und Verlags GmbH, August-Bebel-Allee 6, D-53175 Bonn
Telephone: +49 02 28 949 02-0 • Fax: +49 02 28 949 02-22
Email: info@uno-verlag.de • Web site: http://www.uno-verlag.de

Hungary
Librotrade Ltd., Book Import, P.O. Box 126, H-1656 Budapest
Telephone: +36 1 257 7777 • Fax: +36 1 257 7472 • Email: books@librotrade.hu

India
Allied Publishers Group, 1st Floor, Dubash House, 15, J. N. Heredia Marg, Ballard Estate, Mumbai 400 001,
Telephone: +91 22 22617926/27 • Fax: +91 22 22617928
Email: alliedpl@vsnl.com • Web site: http://www.alliedpublishers.com

Bookwell, 24/4800, Ansari Road, Darya Ganj, New Delhi 110002
Telephone: +91 11 23268786, +91 11 23257264 • Fax: +91 11 23281315
Email: bookwell@vsnl.net • Web site: http://www.bookwellindia.com

Italy
Libreria Scientifica Dott. Lucio di Biasio “AEIOU”, Via Coronelli 6, I-20146 Milan
Telephone: +39 02 48 95 45 52 or 48 95 45 62 • Fax: +39 02 48 95 45 48

Japan
Maruzen Company, Ltd., 13-6 Nihonbashi, 3 chome, Chuo-ku, Tokyo 103-0027
Telephone: +81 3 3275 8582 • Fax: +81 3 3275 9072
Email: journal@maruzen.co.jp • Web site: http://www.maruzen.co.jp

Korea, Republic of
KINS Inc., Information Business Dept. Samho Bldg. 2nd Floor, 275-1 Yang Jae-dong SeoCho-G, Seoul 137-130
Telephone: +02 589 1740 • Fax: +02 589 1746
Email: sj8142@kins.co.kr • Web site: http://www.kins.co.kr

Netherlands
Martinus Nijhoff International, Koraalrood 50, P.O. Box 1853, 2700 CZ Zoetermeer
Telephone: +31 793 684 400 • Fax: +31 793 615 698 • Email: info@nijhoff.nl • Web site: http://www.nijhoff.nl

Swets and Zeitlinger b.v., P.O. Box 830, 2160 SZ Lisse
Telephone: +31 252 435 111 • Fax: +31 252 415 888 • Email: infoho@swets.nl • Web site: http://www.swets.nl

New Zealand
DA Information Services, 648 Whitehorse Road, MITCHAM 3132, Australia
Telephone: +61 3 9210 7777 • Fax: +61 3 9210 7788
Email: service@dadirect.com.au • Web site: http://www.dadirect.com.au

Slovenia
Cankarjeva Zalozba d.d., Kopitarjeva 2, SI-1512 Ljubljana
Telephone: +386 1 432 31 44 • Fax: +386 1 230 14 35
Email: import.books@cankarjeva-z.si • Web site: http://www.cankarjeva-z.si/uvoz

Spain
Díaz de Santos, S.A., c/ Juan Bravo, 3A, E-28006 Madrid
Telephone: +34 91 781 94 80 • Fax: +34 91 575 55 63 • Email: compras@diazdesantos.es
carmela@diazdesantos.es • barcelona@diazdesantos.es • julio@diazdesantos.es
Web site: http://www.diazdesantos.es

United Kingdom
The Stationery Office Ltd, International Sales Agency, PO Box 29, Norwich, NR3 1 GN
Telephone (orders): +44 870 600 5552 • (enquiries): +44 207 873 8372 • Fax: +44 207 873 8203
Email (orders): book.orders@tso.co.uk • (enquiries): book.enquiries@tso.co.uk • Web site: http://www.tso.co.uk

On-line orders:
DELTA Int. Book Wholesalers Ltd., 39 Alexandra Road, Addlestone, Surrey, KT15 2PQ
Email: info@profbooks.com • Web site: http://www.profbooks.com

Books on the Environment:
Earthprint Ltd., P.O. Box 119, Stevenage SG1 4TP
Telephone: +44 1438748111 • Fax: +44 1438748844
Email: orders@earthprint.com • Web site: http://www.earthprint.com

United Nations (UN)
Dept. I004, Room DC2-0853, First Avenue at 46th Street, New York, N.Y. 10017, USA
Telephone: +800 253-9646 or +212 963-8302 • Fax: +212 963-3489
Email: publications@un.org • Web site: http://www.un.org

United States of America
Bernan Associates, 4611-F Assembly Drive, Lanham, MD 20706-4391
Telephone: 1-800-865-3457 • Fax: 1-800-865-3450
Email: order@bernan.com • Web site: http://www.bernan.com

Renouf Publishing Company Ltd., 812 Proctor Ave., Ogdensburg, NY, 13669
Telephone: +888 551 7470 (toll-free) • Fax: +888 568 8546 (toll-free)
Email: order.dept@renoufbooks.com • Web site: http://www.renoufbooks.com

Orders and requests for information may also be addressed directly to:

Sales and Promotion Unit, International Atomic Energy Agency
Vienna International Centre, PO Box 100, 1400 Vienna, Austria
Telephone: +43 1 2600 22529 (or 22530) • Fax: +43 1 2600 29302
Email: sales.publications@iaea.org • Web site: http://www.iaea.org/books